FLUX MEASUREMENTS OF VOLATILE ORGANIC COMPOUNDS FROM AN URBAN TOWER PLATFORM IN HOUSTON, TEXAS: TRENDS AND TRACERS

A Thesis

by

MARTIN CHARLES HALE

Submitted to the Office of Graduate and Professional Studies of
Texas A&M University
in partial fulfillment of the requirements for the degree of

MASTER OF SCIENCE

Chair of Committee,	Gunnar W. Schade
Committee Members,	Renyi Zhang
	Qi Ying
Head of Department,	Ping Yang

May 2014

Major Subject: Atmospheric Sciences

ABSTRACT

Energy and trace gas fluxes were measured from anthropogenic and biogenic emission sources in the Houston urban surface layer. Air sampling from a tall tower platform began in 2008 and continued through April 2013. A relaxed eddy accumulation (REA) system combined with a dual channel GC-FID was used to measure the flux of 19 different volatile organic compounds (VOCs) from C4 through C8 species. We discuss a time series comparison of local concentrations and fluxes of benzene, toluene, ethylbenzene, and xylenes (BTEX) from winter 2009 compared to spring 2013. Median concentrations over the four-year period fell between 20 to 34 percent, comparable to long-term VOC reduction trends observed in other major metropolitan areas. Emissions of these species fell accordingly with median flux reductions of 25 to 54 percent. For emissions inventory validation purposes, traffic counts were taken along major commuter roads surrounding the tower. We observed a strong correlation between selected vehicle exhaust VOC fluxes and traffic counts except during variable working hours.

To assign measured fluxes to local sources, we tested a bulk flux footprint model (Kormann and Meixner model) designed for uniform emission surface areas in this urban, heterogeneous landscape. Tracer releases of known amounts of acetone and methyl-ethyl-ketone (MEK) were performed within the footprint region to validate the model. Four out of six tracer releases matched the fluxes measured at the GC within the given levels of uncertainty for the footprint model and the REA GC-FID system. There

were reasonable causes of error for the two releases that did not match. The footprint model was also tested using a known n-pentane emissions source approximately one mile SSE of the tower. Using modeled footprints under wind directions directly from this source, we calculated that the facility emitted an average of 6.35 ± 3.63 (1 sd) kg of n-pentane per hour. These rates fell within the facility's TCEQ permitted hourly emissions allowing 10.5 kg of VOC per hour. However, if occurring daily, the calculated emission would be above the permit's yearly emission rate of 4.67 kg of VOC per hour at a 68% likelihood based on a normal distribution.

DEDICATION

This thesis is dedicated to my family, friends, and coworkers. Thank you for all the support and encouragement you have given me throughout my undergraduate and graduate years. The environment you have created made this an enjoyable and memorable learning experience.

ACKNOWLEDGEMENTS

First and foremost, I would like to thank my advisor, Dr. Gunnar Schade for his support, mentorship, and guidance throughout my career at Texas A&M University. He was always quick to answer my countless questions and helped me develop a passion for atmospheric chemistry. I truly appreciate the opportunity to work on this novel and fascinating research project that has provided me with valuable knowledge and skills that I can apply in my professional career.

Thanks are also due to the rest of my research group, especially Nick Werner, who, in addition to being a great friend and research colleague, has helped me out with many parts of my research including EdiRe, graphing in R, calibrating instruments in Houston, and tracer releases.

I would also like to thank the members of my graduate committee, Dr. Renyi Zhang and Dr. Qi Ying, for their service reviewing my thesis, and all of their thoughts and suggestions regarding my work.

Finally, I would like to thank my family and friends who have made my time in College Station at Texas A&M a pleasant and enjoyable experience. I truly would not be in this position without their support.

TABLE OF CONTENTS

Page

LIST OF FIGURES

Page

LIST OF TABLES

1. INTRODUCTION AND LITERATURE REVIEW

Air quality studies primarily focus on the concentration of EPA criteria pollutants or air toxics with near ground level monitoring and numerical modeling, including inferring emission rates from models using meteorological data as input. But true emission rates may be better assessed by "top-down" measurements of flux instead of concentration. The pollutant flux can be used to validate an emissions inventory in order to understand real atmospheric pollutant dynamics and help evaluate current photochemical modeling schemes. Flux measurements of Volatile Organic Compounds (VOCs), including typical ozone formation precursors such as alkenes, have been routinely accomplished with various micrometeorological techniques, including eddy covariance, disjunct eddy covariance, and relaxed eddy accumulation (REA) over forests and other rural homogenous landscapes (Ciccioli et al., 2003; Gallagher et al., 2000; Olofsson et al., 2003; Rinne et al., 2008; Warneke et al., 2002), but few flux measurements have targeted complicated urban heterogeneous environments (Kota et al 2014; Langford et al., 2009; Langford et al., 2010; Park et al., 2010; Velasco et al., 2005; Velasco et al., 2009). While only 5% of North America is classified as urban land cover, there is a dearth of pollutant flux measurements in urban areas which contain roughly 75-80% of the North American population (Pataki et al., 2006). This is surprising considering that urban air pollution poses significant direct and indirect effects to human health as well as local and regional atmospheric chemistry.

Pollution sources in urban areas are related to man-made structures, anthropogenic activities, and multiple land-uses including natural and introduced vegetation that make up the urban fabric. In order to measure pollutant fluxes over urban terrain, a tall structure must be in place that does not influence the wind itself while allowing a measurement setup. Air sampling should occur at a minimum of twice the urban canopy height and ideally higher to avoid the urban roughness layer (Roth, 2000) and survey an integrated effect from an upwind footprint area. These conditions have limited such studies to a few cities: Velasco et al. (Velasco et al., 2009) measured VOC and CO_2 fluxes in Mexico City in 2006, Langford and coworkers took detailed VOC flux measurements from urban Manchester (Langford et al., 2009) and London (Langford et al., 2010), and Park et al. performed multiple pollutant and VOC fluxes in Houston in 2008 and 2009 (Park et al. 2010).

While improvements have been made in recent years, air quality with respect to ground level ozone and particulate matter remains poor in Houston, Texas, the 4th largest metropolitan area in the United States. Ground level ozone concentrations are regularly in violation of the National Ambient Air Quality Standard (NAAQS) during April through October (Banta et al., 2005). Several factors contribute to Houston's nonattainment of ozone concentrations, including the largest number of petrochemical facilities in the US, significant precursor emissions within the highly urbanized Houston-Galveston Bay (HGB) area, high ozone production rates, complex interactions between land-sea breeze circulations, and potential pollution transport from domestic and international source regions (Daum et al., 2003; Daum et al., 2004; Vizuete et al. 2011).

The EPA forecasts that Harris County, in which Houston is located, will likely remain in violation of the 2008 8-h NAAQS ozone standard of 75 ppb by the year 2020 (2008 Standards for Ground-Level Ozone, http://www.epa.gov/air/ozonepollution/actions.html), indicated in Figure 1.1.

Figure 1.1. Map of counties with monitors projected to violate the 2008 8-hour ozone standard of 75 ppb in 2020.
(http://epa.gov/air/ozonepollution/pdfs/2008_03_monitors_projected_violate_2020.pdf)

Commonly emitted VOCs include alkanes, alkenes, ketones, aldehydes, and aromatics. Anthropogenic VOC sources include vehicle tailpipe exhaust, petroleum processing, transport and evaporation, energy and heat generation, industrial emissions, solvents and paints, and residential aerosol products. Biogenic sources are dominated by higher plants emitting primarily isoprene and monoterpenes. VOCs are precursors to ozone and secondary organic aerosol (SOA) formation. In addition, some VOC's can be harmful to human health at typical ambient urban concentrations. Long-term exposure to aromatic VOCs such as Benzene, Toluene, Ethylbenzene, and Xylenes (BTEX) can cause peripheral neuropathy and toxic encephalopathy, such as memory loss and impaired cognition (Baker et al., 1985) and auditory neuropathy (Draper and Bamiou, 2009). Benzene itself is known as a human carcinogen (Mehlman, 1990; Whitworth et al., 2008). BTEX species are the most abundant aromatic components of VOCs in the atmosphere stemming from vehicle exhaust, gasoline evaporation and solvent usage, and play an important role in atmospheric chemistry as precursors for tropospheric ozone and secondary organic aerosol (SOA) formation as they have higher oxidation rates than alkane species (Atkinson, 1990; Henze et al., 2008; Kelly et al., 2010; Vlasenko et al., 2009). While aromatic and alkene VOC species have a higher contribution to ozone and SOA formation per molecule, alkane VOC species compose the majority of VOCs emitted and thus by mass also have a significant impact on ozone and SOA formation. Due to the health effects of ozone exposure, limiting ozone precursor emissions has been a priority since the 1970s. Mitigation activities, such as through reformulated gasolines and the catalytic convertor, have typically focused on limiting VOC emissions due to

their often dominating effect on ozone production rates in urban areas (VOC limitation). In addition, long term VOC concentrations measured by Warneke et al. (2012) from the Burbank CARB network in the Los Angeles basin from 1990 to 2008 and 2001 to 2008 (Warneke et al. 2012) and von Schneidemesser et al. in London from 1998 to 2008 (von Schneidemesser et al. 2010) show significantly larger reductions in aromatic VOC emissions than alkane emissions. This trend stresses the importance of alkane atmospheric chemistry into the future as alkane VOCs are becoming a larger source of total VOC emissions thus trending toward greater contribution to ozone and SOA formation.

To continue assisting the state of Texas in the assessment of the greater Houston area air pollutant emissions and emission inventories, air pollutant measurements continued through April 2013 from the tall flux tower installation established by Park et al. (2010). The objective was to continue measuring criteria pollutant and VOC fluxes to establish long-term pollutant trends that evaluate the appropriateness of current emission inventories particularly for traffic emissions and a bulk flux footprint model. We introduce geographical, meteorological and traffic conditions at the study site (3 km north of downtown Houston) in section 2, in addition to the methodology for the flux measurements using a REA technique and gas chromatography flame ionization detection (GC-FID). In section 3, we compare the flux measurements from Park et al. during January 2009 from the same research site to recent measurements taken during March and April 2013. In section 4, we compare local traffic counts and local gasoline samples to selected VOC flux measurements. In section 5, we evaluate the application of

a bulk emissions footprint model with VOC tracer releases and the emissions of a local n-pentane source upwind of the tower setup to the fluxes measured at the tower.

2. METHODOLOGY

2.1 Site Description

To monitor neighborhood scale pollutant fluxes, micrometeorological instruments were installed on a tall communications tower in a mixed land use area, approximately 3 km north of downtown Houston, Texas, in spring 2008. The location of the tower (29°47’22” N, 95°21’13” W) is on private property, owned by the Greater Houston Transportation Company (hereinafter called *Yellow Cab*). It is surrounded by residential areas to the North, West and South comprising 28% of the total area within a 1.5 km radius, a light industrial area to the East and immediately surrounding the tower (11%), and Moody Park to the West (6%), Figure 2.1. The remaining land use is comprised of commercial and public land (5% each), undeveloped land (17%), and the remainder consisting of roads and other land uses. The major traffic axes are two multilane, north-south oriented commuter roads approximately 200 m east (Elysian Rd./Hardy Rd.) and 700 m west (Fulton St./Irvington Blvd.), and a smaller two-lane commuter road (Quitman St.) 650 m south of the tower. The area’s urban vegetation is dominated by mature trees, with a slight variation in density with wind direction (Park et al., 2010).

---

*Reprinted with permission from “Flux Measurements of Volatile Organic Compounds from an Urban Tower Platform” Changhyoun Park, 2010. Texas A&M University Libraries Repository.

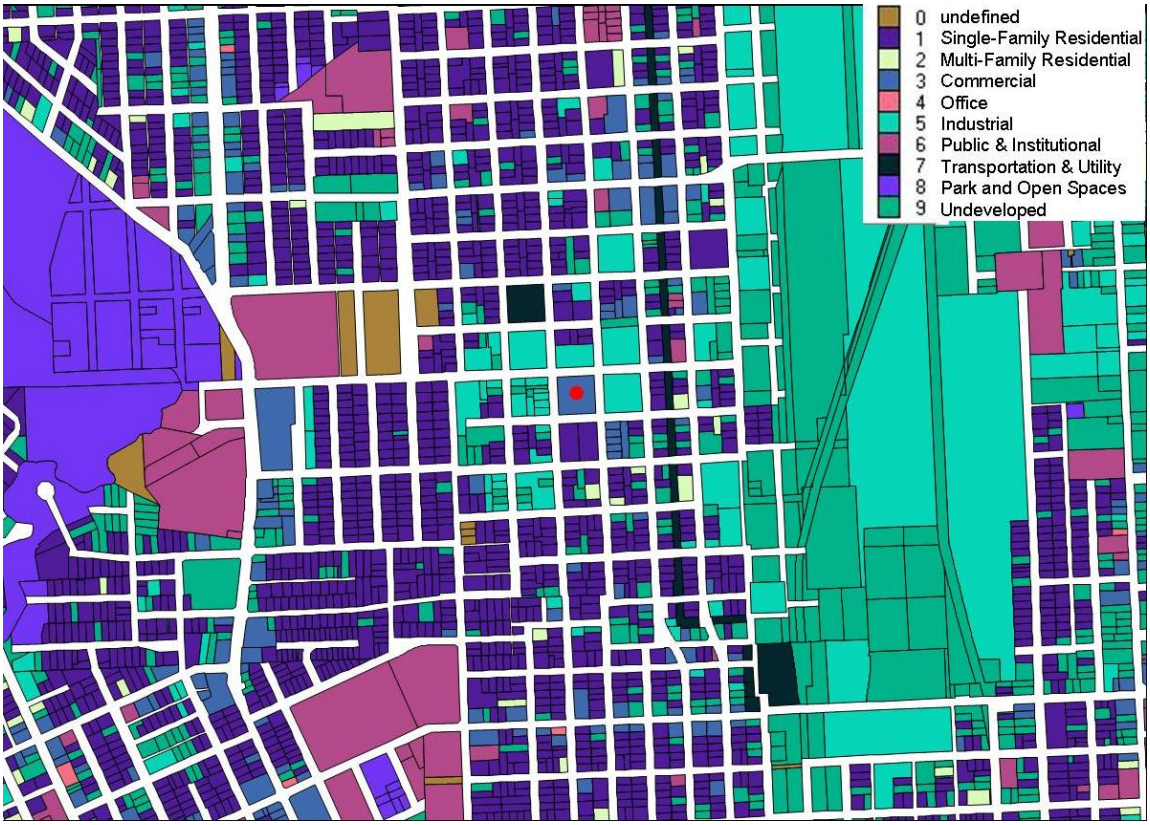

Figure 2.1: Map of land usage surrounding the Yellow Cab flux tower (red dot). Extension from tower ≈ 1 km.

2.2 Meteorological Data and Traffic Counts

The flux data used in this study is from two different time periods. The first period occurred from December 5 – 11, 2011, February 2 – 17, 2012, and February 22 – March 4, 2012, and hereinafter will be called the winter 2012 period. The second period occurred from March 11 – April 20, 2013, and hereinafter will be called the spring 2013 period. Meteorological observations during these periods are summarized in Figure 2.2.

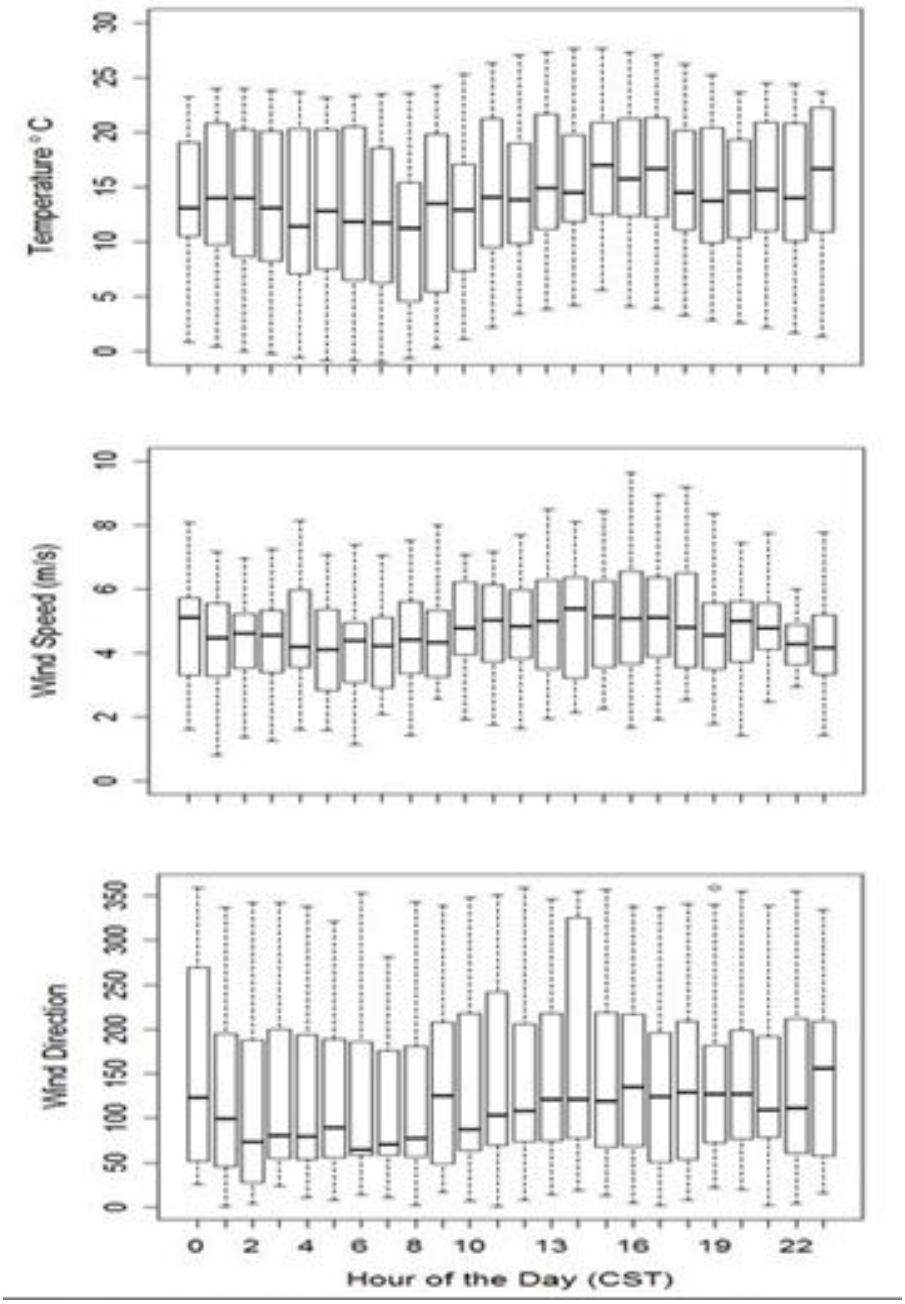

(a)

Figure 2.2: Boxplots of the diurnal variation of meteorological conditions during the (a) winter 2012 and (b) spring 2013 study period. Solid black bars are medians, gray boxes are inter-quartile ranges (IQR) and whiskers represent 95% intervals with individual points indicating outliers outside 97.5% of the data. CST is central standard time and CDT is central daylight saving time.

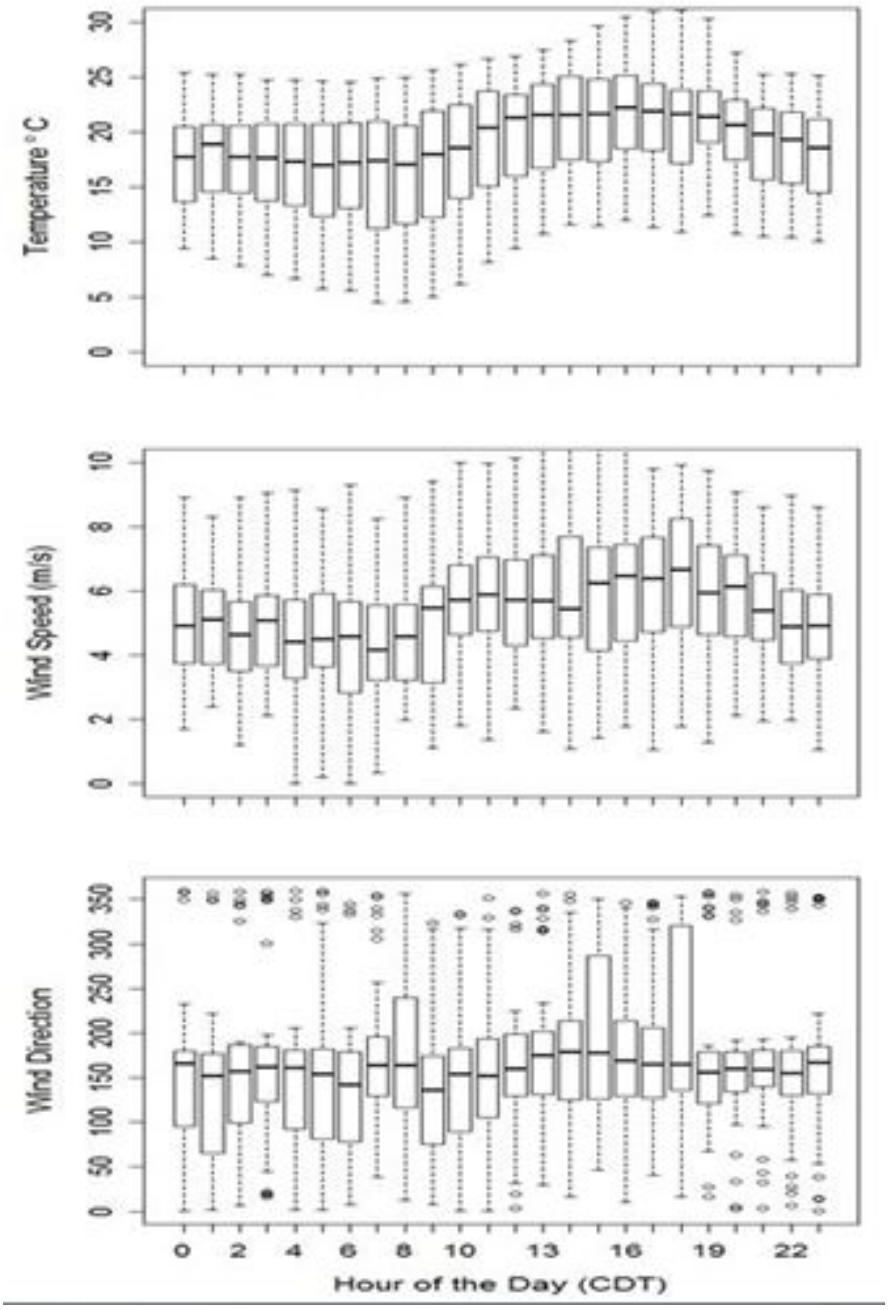

(b)

Figure 2.2: Continued.

Temperature changes between frontal passages typical for the cool season in Texas varied greatly during both periods (as indicated by large IQRs) with an average temperature of 14.8 °C and 18.6 °C during the winter 2012 and spring 2013 periods respectively. Temperatures were at their lowest immediately after sunrise and peaked in the late afternoon. Following temperature-driven boundary layer development, the lowest wind speeds occurred during the morning boundary layer transition, then continually increased, maximizing in the early afternoon hours for the winter 2012 period and early evening for the spring 2013 period. Spring 2013 showed a larger diurnal variation in wind speed. Both periods rarely observed westerly winds (225°-315°) with a 3% and 2% occurrence in winter 2012 and spring 2013 respectively. While we observed 36% northerly winds, 35% easterly winds and 26% southerly winds for the winter 2012 period, we observed a greater occurrence of southerly winds at 56% with 24% northerly winds, and 18% easterly winds during the spring 2013 period.

Figure 2.3 shows average weekday traffic counts for Hardy/Elysian, Collingsworth, Loraine, Hays, Quitman, and Luzon Streets. Hardy/Eylsian Streets are major multi-lane commuter roads, Collingsworth, Loraine, Hays, and Quitman Streets are smaller 2-lane commuter roads, and Luzon Street is a typical neighborhood road in the study area. These roads are highlighted in Figure 2.4. Hardy/Elysian, Loraine, and Luzon Street counts were gathered from June 26 – July 13, 2012, Quitman and Hays Street counts were gathered from March 29 – April 11, 2011, and Collingsworth Street counts were gathered from November 16 – 29, 2011 all using rubber tube technology (courtesy of the Texas Transportation Institute, TTI). These vehicle counts demonstrate

that the highest number of vehicles passed through the study domain during morning and evening rush hours, especially for the major Hardy/Elysian commuter road, with a more prominent evening rush hour and elevated traffic counts during the daytime and afternoon hours versus nighttime hours. In addition, Hays and Quitman counts displayed early afternoon school traffic peaks from the local elementary, intermediate, and high schools in the area while other streets had slightly elevated lunch-hour peaks around noon.

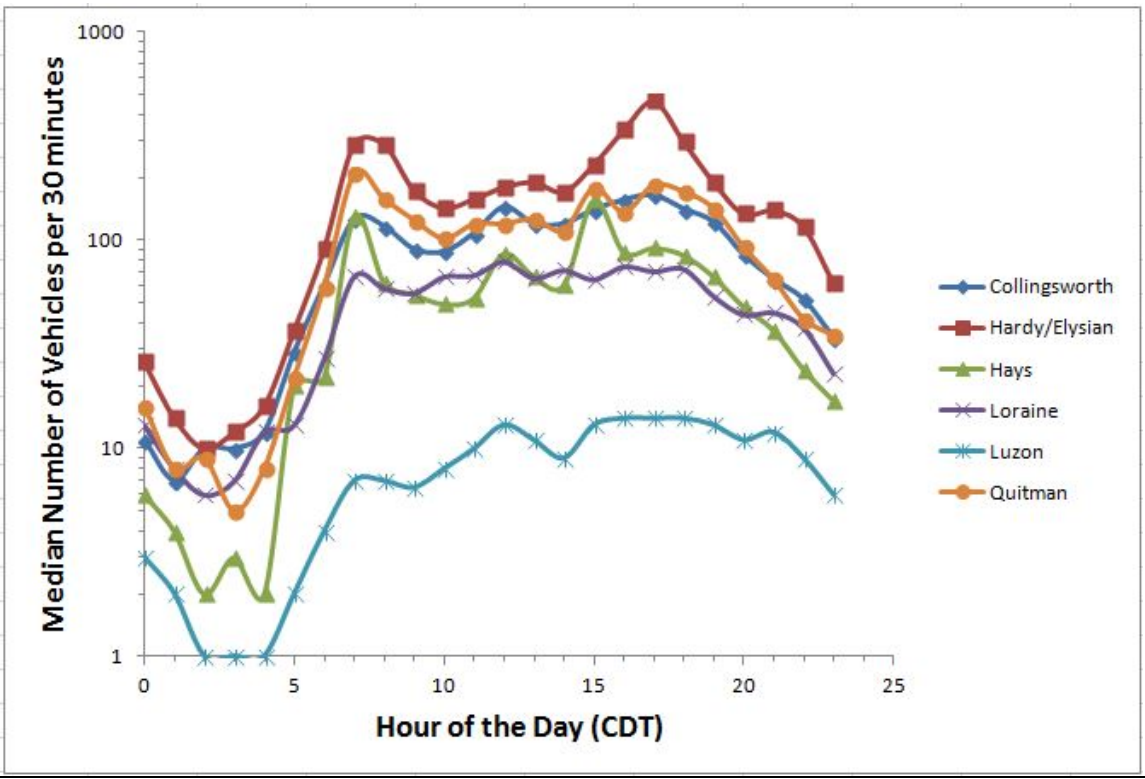

Figure 2.3: Median diurnal number of vehicles in 30 minute intervals (logarithmic y-axis) obtained during approximate two-week periods on weekdays between April 2011 – July 2012 for streets within the footprint region including a major multi-lane commuter road (Hardy/Elysian), smaller 2-lane commuter roads (Collingsworth, Hays, Loraine, and Quitman), and a typical neighborhood street (Luzon).

Figure 2.4: Map of the study area with streets highlighted in blue where traffic counts were taken and Yellow Cab parking lots highlighted in orange.

The Yellow cab company has multiple parking lots as seen in Figure 2.4 with a high daily traffic flow of cabs and personal vehicles. As evaporative and idling emissions from cars in areas directly surrounding the tower could have a significant

contribution to local VOC emissions, we wanted to have a better estimate of this emissions source by taking hourly parked and running car counts within the Yellow cab lots. Figure 2.4 shows the counts of parked and idling or running cars in the Yellow cab parking lots from 07:15 through 19:15 CDT on September 17, 2013, a typical weekday for the company, with counts occurring from the 15 to 25 minute mark of every hour for consistency.

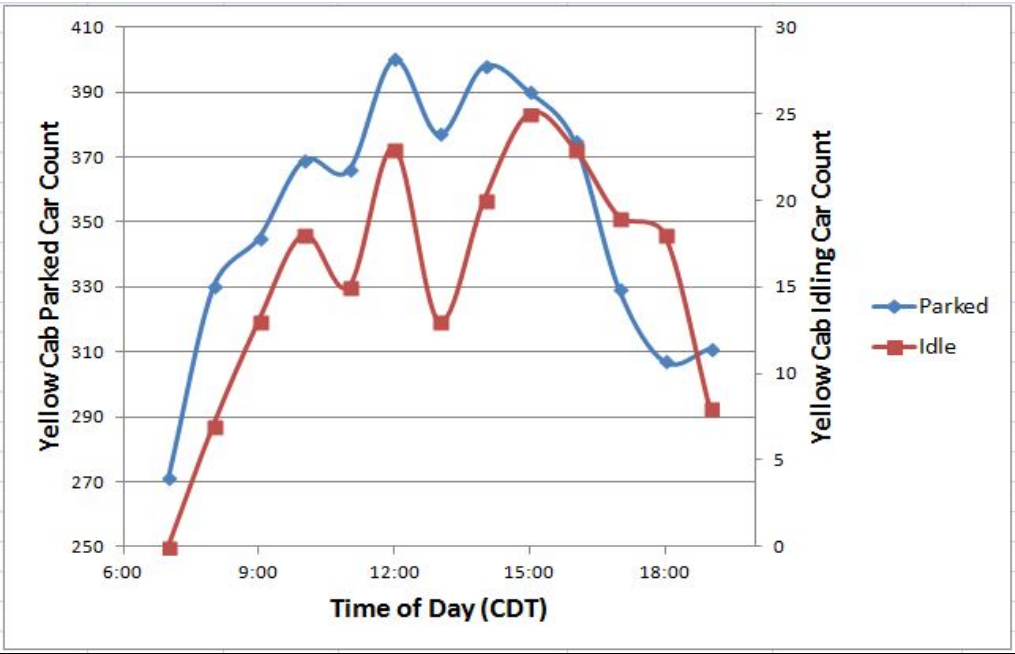

Figure 2.5: Parked and Idling car counts in Yellow Cab lots from 07:15 through 19:15 central daylight saving time (CDT) on September 17, 2013.

The company had a minimum of 271 cars parked in the early morning hours with afternoon maxima from 12:15 – 15:15. There were no idling cars in the morning, but increasing idling counts with a maximum in the late afternoon hours of up to 25 cars

idling at 15:15. In section 3.2, we will compare local area traffic counts and Yellow Cab parked and idling car counts to measured fluxes from the spring 2013 period.

2.3 VOC Measurement System and Quality Control

2.3.1 Sample flow path

Yellow Cab owns and operates a 91 m tall, 60 cm side length, triangular lattice communications tower on one of the parking lots on its property. Meteorological sensors for temperature, relative humidity, and wind speed were installed at four heights on the tower up to a height of 60 m in May 2007, and then upgraded by an additional level in 2008. The flux measurement set up at the top installation height of 60 m consisted of additional radiation sensors and a southward facing sonic anemometer for 3-D wind speeds (CSAT3, Campbell Scientific Inc. (CSI), Logan, UT) monitored by a CR1000 data logger (CSI). A 9.5 mm OD Teflon PFA tubing inlet was installed from the top level next to the sonic anemometer, down the tower, across a short cable track, and into a small air-conditioned building at its base (Figure 2.5). Ambient air was sampled down the PFA tubing into the building at approximately 17.3 L min^{-1} via a rotary vane pump to where the GC-FID, a CO_2/H_2O analyzer (LI7000, Licor Biosciences, Lincoln, NE), and criteria air pollutant instrumentation for CO, NO_x, and ozone were located. A 2 µm pore size Teflon PTFE filter located at 3 m above the ground on the tower was used to remove particulates from the air stream before it reached the gas analyzers. This filter was changed approximately every 10 days during routine checks and calibrations to

ensure a stable air flow and line pressure. For VOC subsampling, a Teflon-coated membrane pump extracted approximately 0.9 L min^{-1} from the main air flow through a ¼" OD Teflon PFA tube with an inline ozone scrubber composed of KI coated glass wool and pushed the subsampled air through a flow controller (PTFE/sapphire ball flow meter with needle valve; Cole-Parmer, Vernon Hills, IL) into the REA valve system used by the GC-FID.

2.3.2 Relaxed Eddy Accumulation (REA) setup

The REA method is an eddy covariance derived sampling method within the atmospheric surface layer, used for trace gases, for which a fast measurement sensor does not exist. The eddy accumulation method was first proposed by Desjardins (Desjardins, 1972), but was later improved by Businger and Oncley (1990) to the relaxed eddy accumulation method. The two basic components required for REA sampling are a fast-response (10 Hz) anemometer measuring the vertical wind speed, and a fast response valve system diverting the sample air depending on the sign of the measured vertical wind speed. Meaning, during an *updraft*, or positive vertical wind speed, the high speed valve opens for the *updraft* sample, and this air enters the *updraft* reservoir.

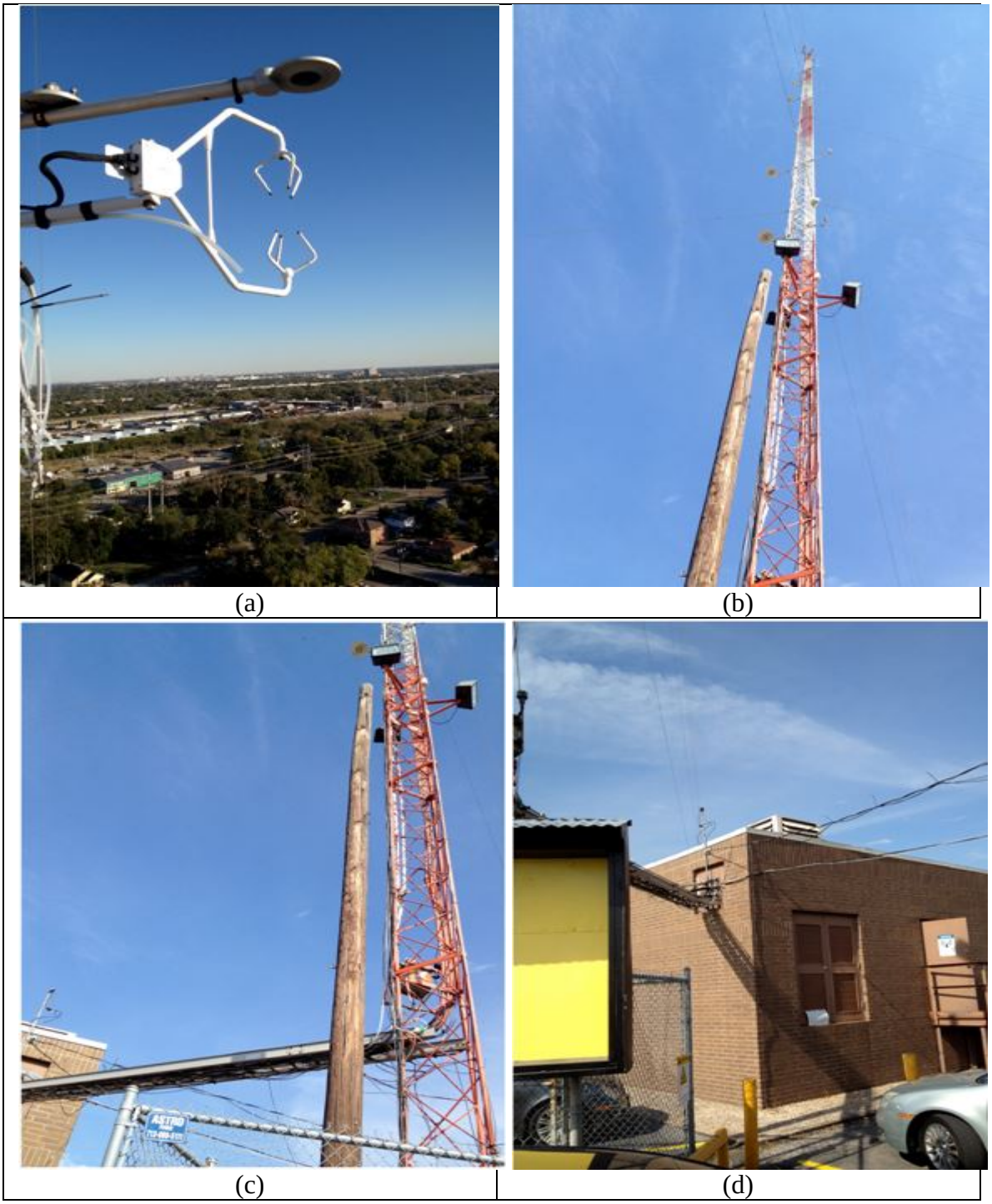

Figure 2.6: Pictures of our tower sampling setup. A 9.5 mm OD Teflon PFA tubing inlet was installed from the top level next to the sonic anemometer (a), down the tower (b), across a short cable track (c), and into a small air-conditioned building at its base (d).

The REA system used in this research project is almost identical to the system operated by Park et al. (2010), consisting of three fast-response two-way valves (model 100T2NC, BioChem Valve Inc., Boonton, NJ; response time < 20 ms), one each for updraft and downdraft sampling, and a 'deadband' that excludes sample air associated with small deviations of the vertical wind speed from its mean. The valves were controlled by the data logger that acquired the instantaneous 3D wind speeds and computed a 10-minute running average of the vertical wind speed (w) and its standard deviation (σ_w) (Schade and Goldstein, 2001). These values were buffered by a lag time of ~8.5 seconds to account for the time it took the air sampled at the 60 m height on the tower to travel to the REA valve system. This lag time was computed offline from the maximum of the w-CO_2 covariance using the acquired 10 Hz data of the CO_2 concentration by the CO_2/H_2O analyzer. Additionally, this lag time correlates well to estimations from flow and volume (2.3 L) calculations.

An updraft or downdraft sample is taken when w exceeded mean(w) ± bσ_w, in which b is a discrimination factor introduced to vary the deadband size, and σ_w is the standard deviation of the vertical wind speed of the preceding 10 min. We used a large b factor of 1.1 that corresponds to a deadband size of approximately 80% to maximize the concentration differences of emitted VOCs in the up and downdraft samples. For our sampling period of 30-minutes, each channel contained approximately 3 minutes of sample per reservoir (10% each) for a total sample size close to 3 L of air per channel based on a flow rate of 0.9 L/min. Our REA system shown in figure 2.5 is unique in that

it can maximize the up and downdraft concentration difference without compromising the sample size, thereby increasing the flux measurement sensitivity.

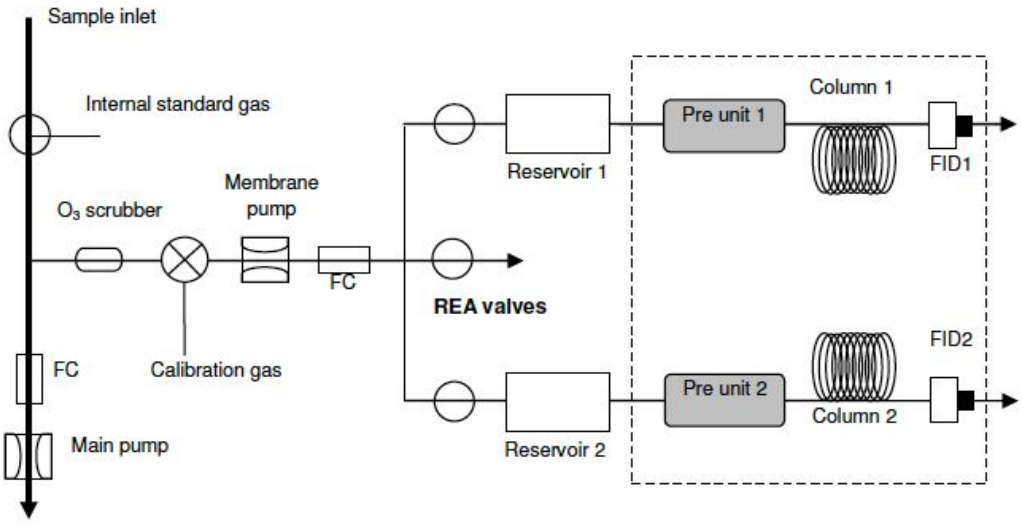

Figure 2.7: Schematic of REA-GC-FID system. The dashed line box indicates the parts of the GC-FID system, with preconcentration units ("Pre Unit") described in more detail in figure 2.7 (Park et al., 2010).

Each VOC flux (F) from the REA system data is calculated using

$$F = \beta\sigma_w(C_{up} - C_{down}) \quad (2.1)$$

where σ_w is the standard deviation of the vertical wind speed over the 30 minute collection period, C_{up} and C_{down} are the concentrations of each compound of interest in the up and downdraft reservoirs respectively, and the β factor is a unitless coefficient with a value of approximately 0.58 in ideal atmospheric turbulence conditions such as over flat, homogenous terrain (Katul et al., 1996). The β factor is generally assumed to be constant, but when a deadband is used, it is calculated from measurements of sensible heat flux and virtual mean air temperatures that correspond to the sampled up and

downdrafts (Businger and Oncley, 1990; Katul et al., 1996; Schade and Goldstein, 2001). By calculating the flux correction β factor, an additional uncertainty is introduced into the REA method. The β factor is thought to depend on atmospheric stability (Ammann and Meixner, 2002; Andreas et al., 1998; Milne et al., 2001; Park et al., 2010) but is generally calculated from the wind speed measurements in an inversion of equation 2.1 such that:

$$\beta = \frac{\overline{w'T'}}{\sigma_w(\overline{T}_{up} - \overline{T}_{down})} \tag{2.2}$$

where the primes denote deviations from the respective mean values. During near neutral atmospheric stability, commonly observed when the sensible heat flux changes signs in the morning and evening hours, differences between the sensible heat flux components T_{up} and T_{down} become very small and create large uncertainties as the denominator in equation 2.2 approaches 0. Baker et al. (1992), Bowling et al. (1998), Park et al. (2010), and Schade and Goldstein (2001) discarded calculated β factors when sensible heat fluxes were small. Here, we used a fixed β factor of 0.335 corresponding to the median of all half-hour values calculated using equation 2.2 from both sampling periods. Median β factors varied less than 5% from the overall median throughout the day, as can be seen in figure 2.6, so one single β value was used for both sampling periods. Even though Park et al. (2010) used a 5-minute running average of w and σ_w for their REA system, while this research used a 10-minute average, our median β factor is within 6% of their median β factor of 0.355, demonstrating the consistency of the REA setup and sampling environment.

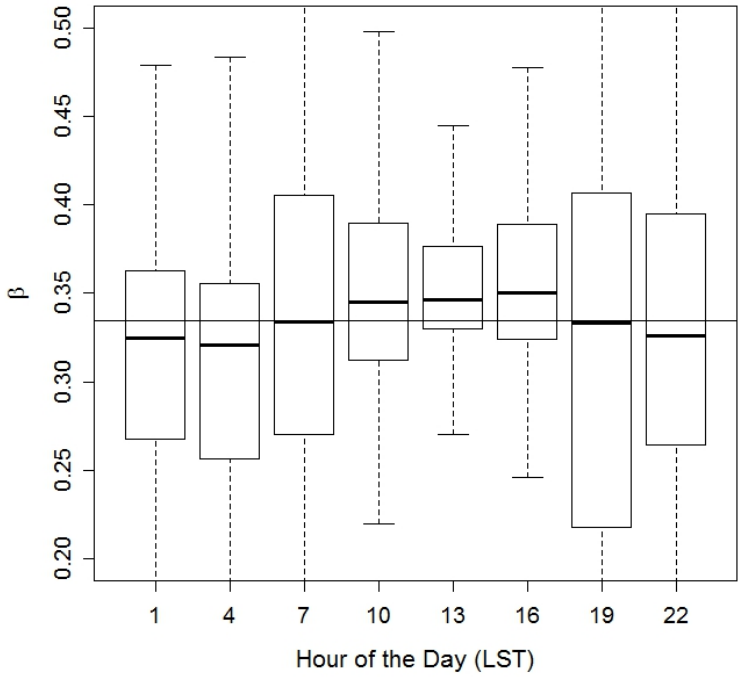

Figure 2.8: Boxplot of diurnal variations of median β factors for 3-hour periods for both sampling periods. The line indicates the median β factor used of 0.335.

2.3.3 GC-FID analysis

The GC-FID system consisted of a portable SRI model 8610 C with dual channel setup (SRI Instruments, Torrance, CA). Each channel had a preconcentration unit, a capillary column with a guard column, and an FID fueled by zero air and hydrogen from onsite generators (AADCO model 737-1 and VWR hydrogen generator model 97001-252), similar to the setup used in Park et al., (2010). Figure 2.9 depicts the preconcentration unit. A single, software-controlled pump aspirated air from 3 L Teflon bags into one each updraft and downdraft preconcentration unit eight minutes offset from the sample acquisition interval for a total sampling time of 30 minutes. The

sampling flow rate was controlled by two flow controllers (AALBORG, Orangeburg, NY) to 100 mL min^{-1}. Each preconcentration unit consists of a 1/8" OD, 10 cm length Silcosteel® adsorption trap filled with 60/80 mesh Carbopak-B (50%), Carbopak-X (30%), and Carboxen 1000 (20%) (all Supelco, PA), and is heated by an insulated resistance wire. After sampling is complete and the GC is ready, each valve rotates in turn, so that during the first 12 seconds of the GC operation, hydrogen used as the carrier gas sweeps each trap consecutively to remove oxygen. Both samples are then thermally desorbed as the insulated resistance wires heat the trap to 190 °C within approximately 18 seconds and stays heated at 190 °C for approximately 1.5 minutes, desorbing the sample directly into one each 0.53 mm ID Rtx-MXT624 column via 10-port Valco® valves and 1/16" OD Silcosteel® tubing 15 minutes after the sample collection ended. Cromatographic data acquisition and GC control are carried out via PeakSimple software (SRI Instruments, Torrance, CA). The GC oven temperature program was set to hold at 30 °C for 10 minutes, then ramp at 4 °C, then ramp again at 20 °C/min to 215 °C. After an additional 9 minutes holding time, the temperature was decreased until the end of the run. The initial carrier gas (H_2) column head pressure setting was 0.5 kPa (7 psi), then ramped in order to provide a near constant flow through the MXT columns. Raw chromatographic data were individually reanalyzed offline for consistency using PeakSimple software set to output area counts to an ASCII file.

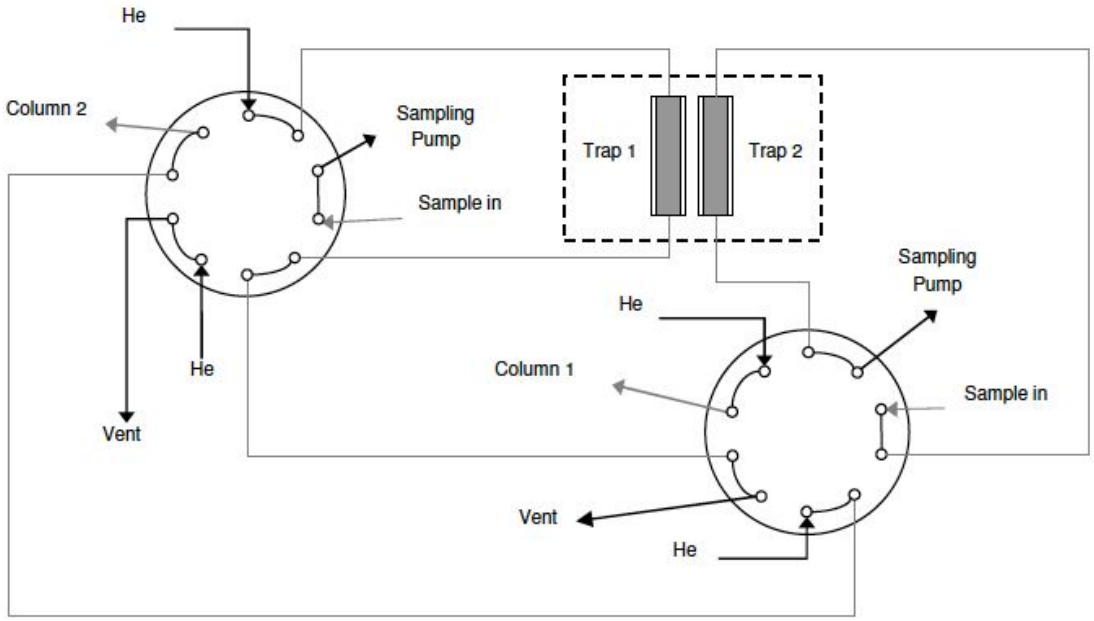

Figure 2.9: Depiction of the preconcentration unit (10-port valves, traps and sampling pumps) as part of the SRI gas chromatograph. All lines in contact with the sample are Silcosteel tubing (grey lines). Both vents are metered with a needle valve to control the H_2 carrier gas flow rate during the trap purge. The dashed line box indicates the heater blocks (Figure unchanged from Park et al., 2010).

2.3.4 Quantification

The GC-FID system had been tested in the laboratory before it was deployed to the *Yellow Cab* research site to determine optimal sample size, breakthrough characteristics, compound elution times, and optimal chromatographic separation. Because the traps operated at room temperature, C_2 hydrocarbons were not, and C_3 hydrocarbons were incompletely trapped. C_4 hydrocarbons were completely trapped at ppb-mixing ratios observed at the *Yellow Cab* site, but were noted to experience minor breakthrough at very high mixing ratios tested in the lab by Park et al. (2010). However, C_3 hydrocarbons and isobutene were not chromatographically separated. Higher

hydrocarbons ($\geq C_5$) were completely trapped up to high ppb mixing ratios (>500 ppb) and generally well separated, except for 2,2,4-trimethylpentane (isooctane) and benzene, which elute at nearly the same time on this 0.53 mm ID Rtx-MXT624 column and thus fall under the same chromatographic peak.

Compound identification is based on retention time as compared to single or multi-species standards injected into zero air standards absorbed by the trap. Due to the high linearity and carbon proportionality of the FID (Ackman, 1968), we used an internal standard (IS) in routine daily field operations. A weighted response factor for each compound was calculated (Ackman, 1964), and the IS's response factor was calculated from dilutions of the ppm-level IS into the main tower line. We used 3-methylheptane as the IS as it was not naturally abundant at the *Yellow Cab* site, well separated on this column, and fully trapped on and released from the preconcentration traps. The response factor of the IS (RF_{IS}) was calculated for the winter 2012 and spring 2013 sample periods based on 421 and 690 samples, respectively, produced by varying the concentration of the IS via at least three dilution ratios within the several weeks of instrument operation during each sampling period. The RF_{IS} was determined from the regression equation from peak area versus concentration for each channel. Individual hydrocarbon response factors (RF) were determined from the mass-%C of the hydrocarbon relative to the internal standard compound (RF_m). Lamanna and Goldstein (1999) showed that the ratio of RF/RF_m is generally close to 1, particularly for hydrocarbons. For this data, we assume that RF_m is representative of the correct response

and we used the derived RF from mass %C relative to the IS to quantify all hydrocarbon species measured in the field. The respective data are summarized in Table 2.1.

Table 2.1: Quantification parameters of selected hydrocarbon compounds

Compound	Blank, ppbv	Derived RRF_i	Ratio RF_{IS}/RRF_i for Spring 2013 period
n-pentane	<LDL	0.618	0.11
n-hexane	<LDL	0.746	0.009
Benzene	<LDL	0.823	0.008
Toluene	<LDL	0.950	0.007
Ethylbenzene	<LDL	1.076	0.006
Xylenes	<LDL	1.076	0.006

Here, <LDL denotes below least detectable limit; RRF_i denotes mass %C weighted response factor for the individual compounds relative to the IS (3-methylheptane); RF_{IS} is the response factor of the IS.

2.3.5 Quality control

For quality control, zero air sampling and channel intercomparison tests were initiated by the data logger every 30 hours. For zero air sampling, a three-way valve located in front of the sample acquisition pump is turned changing the sample flow from ambient air to zero air provided by the zero air generator. Zero air sampling also occurred during rain events, because the large main line sampling pump was turned off in these conditions in order to avoid water entering the sampling line.

The room in which the instruments were located housed a bottle of n-butanol (for a local condensation particle counter) with a small vent hole in the bottle that created elevated concentrations of n-butanol in the room. Therefore, when large n-butanol peaks

were observed in the chromatographic data, it was indicative of a leak in the system signifying the sample had been compromised and was generally unusable.

The IS integrated area ratio between the two channels for every sample was multiplied to each hydrocarbon measured in the downdraft channel because the updraft channel almost always contained a larger sample size. This uneven sample size is thought to be attributed to an uneven flow resistance between the updraft and downdraft valves in the REA system and the up and downdraft biases caused by the local atmospheric turbulence in a given half-hour sample. Also, channel intercomparisons were done with a 10-hour offset from zeroing by opening and closing the updraft and downdraft valves simultaneously, thereby acquiring identical samples into the bags. The comparison of these samples makes it possible to monitor channel offsets as caused by the sampling and analysis system (Schade and Goldstein, 2001). We selected 19 single hydrocarbons out of these channel intercomparison samples to determine the slope of the average channel ratio and then multiplied the updraft channel by the slope of the intercomparison.

Manually verifying each chromatogram also presented another method of quality control as integration errors were often noticed under programmed, automatic integration. Most integration errors were attributed to occasional, uneven peak shape between the up and downdraft chromatograms as well as to varying ambient temperatures in the room housing the instrument causing shifts in retention time. An example is given in Figure 2.10.

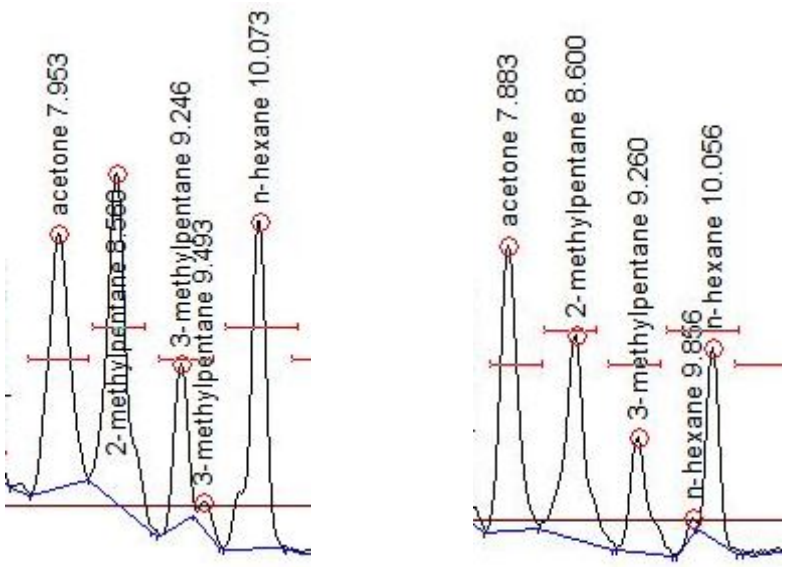

(a) (b)

Figure 2.10: Sample updraft (a) and downdraft (b) chromatograms from the same hour presenting differences in automatically integrated peak shape in both 3-methylpentane and n-hexane.

3. RESULTS

3.1 Long-term Trends in BTEX Concentrations and Fluxes

We discuss the results of measured concentrations and fluxes of the BTEX species measured during the winter 2012 and spring 2013 sampling periods and compare these results to those measured by Park et al. (2010) from the same site utilizing an almost identical set up. For quality assurance, only flux data acquired under sufficiently turbulent atmospheric conditions, in this case a friction velocity (u*) exceeding 0.20 m s^{-1}, were retained. The u* filter removed 17% of flux data from the winter 2012 period and 22% of flux data from the spring 2013 period.

The observed BTEX concentration patterns, Figures 3.1 and 3.2, exhibited typical trends expected in an urban area: a noticeable weekday morning rush hour peak followed by a drop and lower daytime than morning abundances due to less vehicle traffic and a higher boundary layer (BL). Due to a deep BL under typical urban heat flux conditions, the mixing layer height is kept high throughout the afternoon and evening hours, thus preventing surface layer VOC emissions from the evening rush hour to accumulate fast. Of interesting note, a weak weekend evening peak was observed, likely due to increased car traffic. Nighttime mixing ratios were generally lower despite lower BL heights because of much reduced nighttime car traffic.

---

*Reprinted with permission from "Flux Measurements of Volatile Organic Compounds from an Urban Tower Platform" Changhyoun Park, 2010. Texas A&M University Libraries Repository.

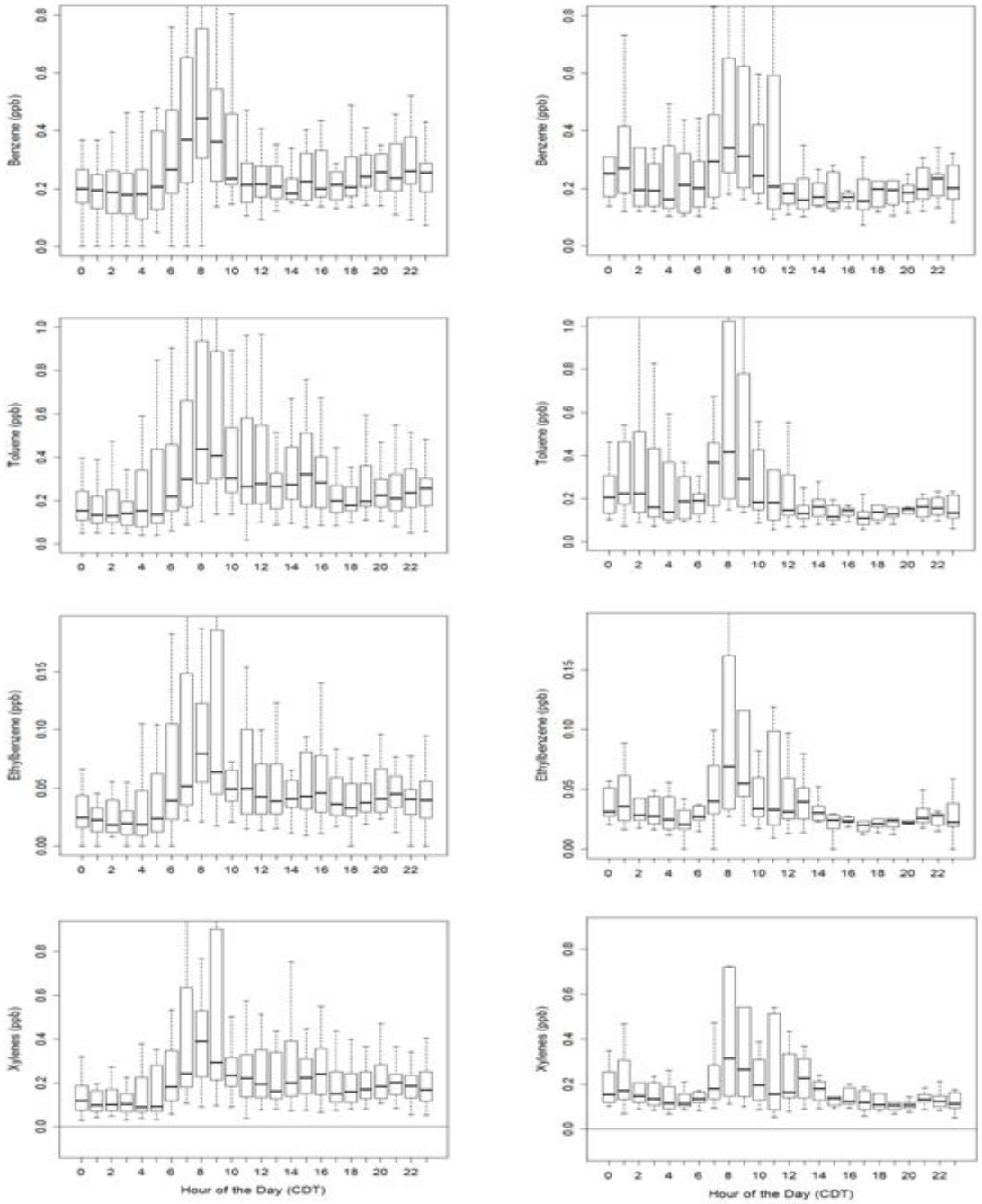

Figure 3.1: Diurnal boxplots of BTEX concentrations in updrafts for all wind directions during the spring 2013 period. Plots on the left hand and right hand side are weekday and weekend data, respectively.

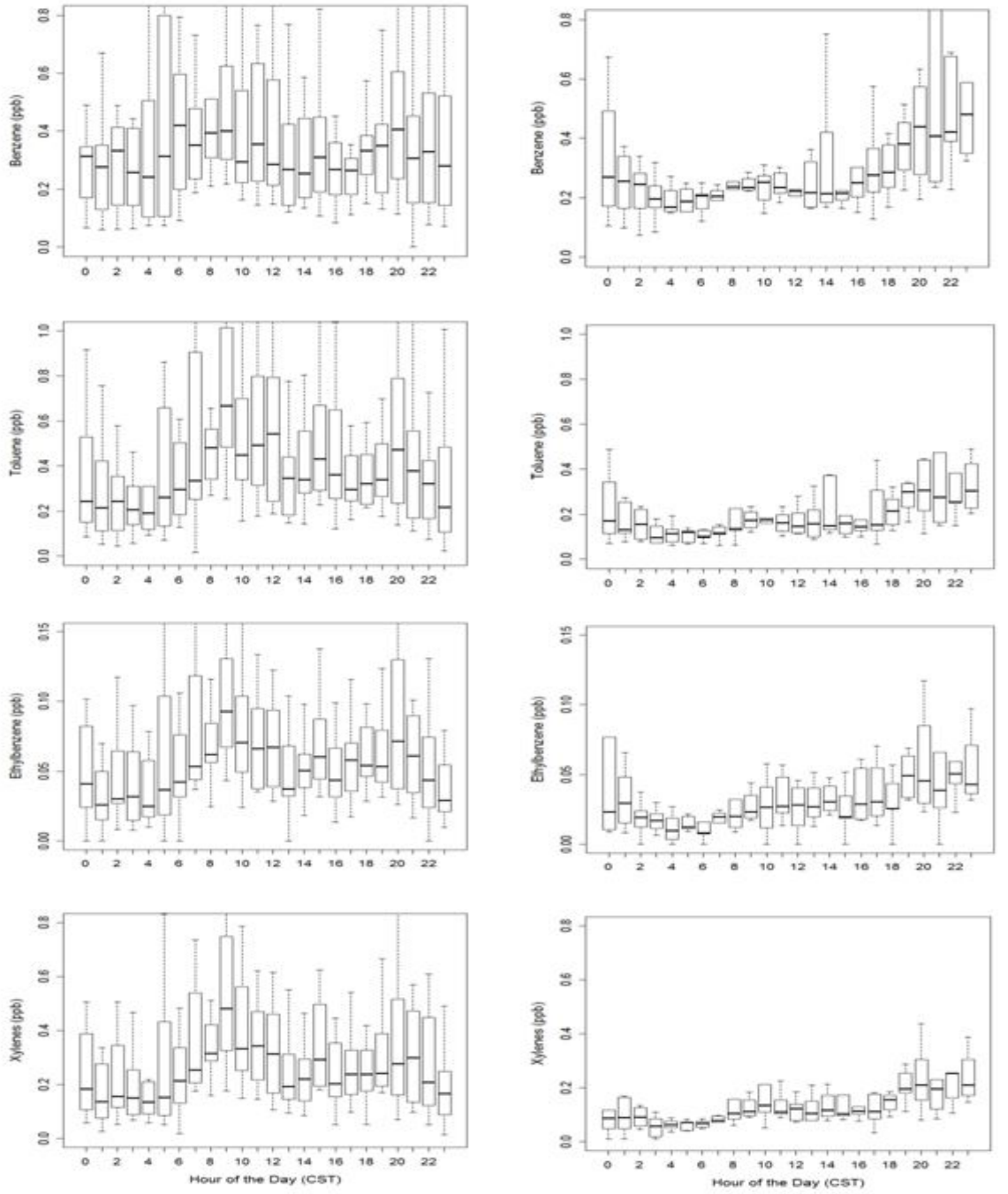

Figure 3.2: Same as Figure 3.1, but for the winter 2012 period.

Boxplots of diurnal flux variations of the BTEX species are shown in figures 3.3 and 3.4 for the spring 2013 and winter 2013 respectively. Overall, the largest fluxes of the BTEX species were from toluene, followed by xylenes, benzene/isooctane, and ethylbenzene. During the weekdays, all BTEX species from both periods showed a distinct morning rush hour peak and afternoon maxima, and minima close to zero median flux during the early morning hours. Weekend BTEX fluxes during the winter 2012 period were significantly lower than weekday fluxes, while only Toluene fluxes were significantly lower on weekends for the spring 2013 period. However, weekend fluxes have significantly fewer data points with 192 and 119 weekend hours versus 498 and 302 weekday hours for the spring 2013 and winter 2012 periods, respectively, such that too few data points potentially bias individual hours on these diurnal boxplots.

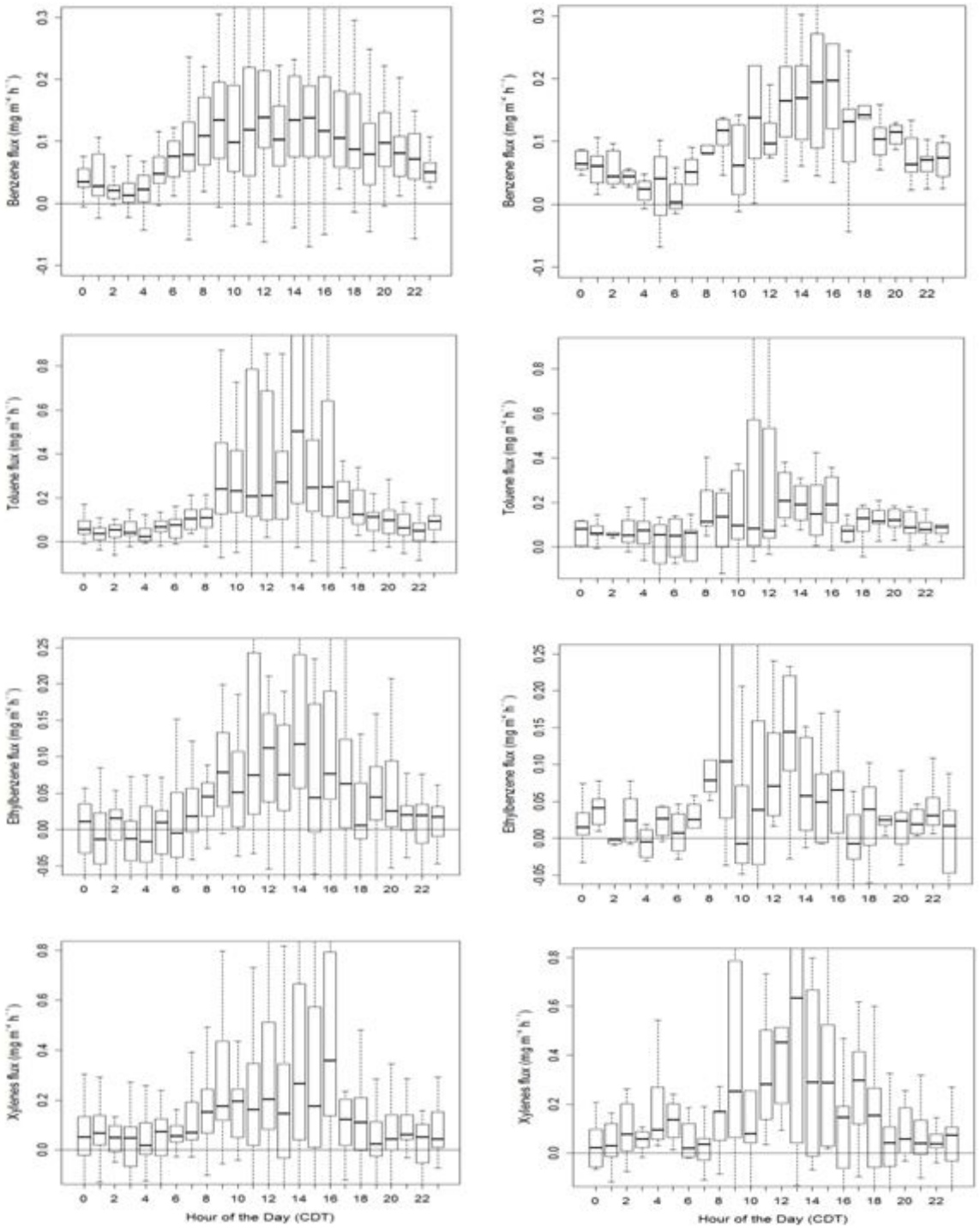

Figure 3.3: Diurnal boxplots of BTEX fluxes for all wind directions during the spring 2013 period. Plots on the left and right side are weekday and weekend data, respectively.

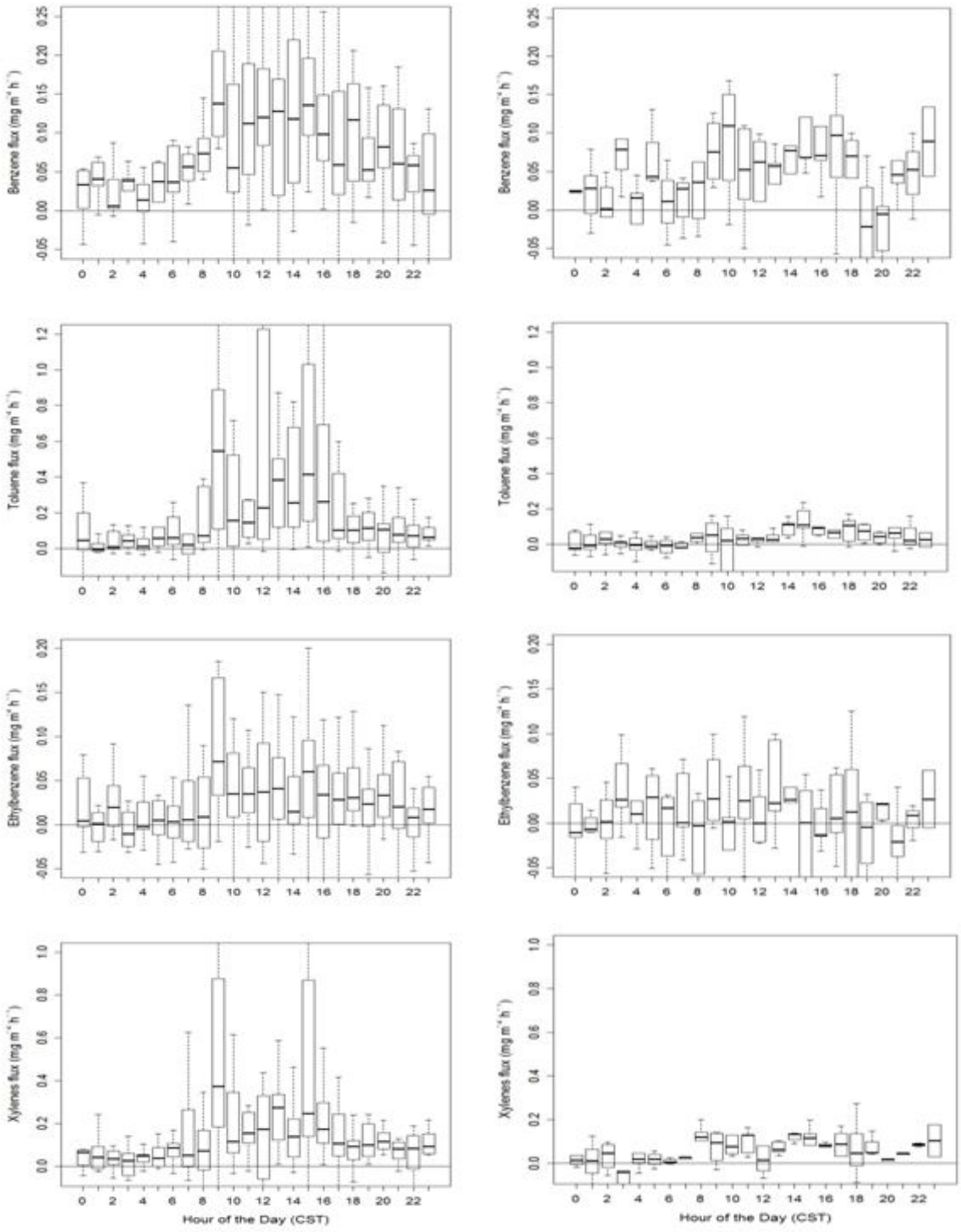

Figure 3.4: Diurnal boxplots of BTEX fluxes for all wind directions during the winter 2012 period. Plots on the left and right side are weekday and weekend data, respectively.

In table 3.1, we compare our concentration results to earlier research performed by Park et al. (2010) from January 1 – February 28, 2009. We decided to compare our datasets only to the previous winter time data set to account for seasonal differences that can cause variations in VOC evaporation rates and regional petroleum consumption. All BTEX species exhibited a significant decline in median concentrations over the past 4 years ranging from 20 to 34 percent. Concentrations of anthropogenically emitted VOCs have long been declining throughout the United States. Data from the Burbank CARB network in the Los Angeles metropolitan area suggests BTEX yearly reductions between 8 to 11.6 percent (Warneke et al., 2012) from 1990 to 2008, while the Houston Regional Monitoring Network showed evidence of an average 85 percent reduction in ambient concentrations of BTEX from 1988 to 2011. In addition, the EPA recently required a reduction in the benzene content of gasoline to a maximum of 0.62%/vol. from 1%/vol for large refineries starting in 2011 (United States Environmental Protection Agency, 2007). Our research shows that this VOC reduction trend was also occurring at the *Yellow Cab* site with comparable average yearly reductions between 5.5 percent for ethylbenzene to 10 percent for toluene. As mentioned in section 2.3.4, it is important to note that our chromatographic benzene peak also contains isooctane, which has proven to be a significant constituent of Houston-area gasoline emissions (McGaughey et al. 2004). However, since Park et al. (2010) defined this same peak entirely as benzene, we also characterized this peak entirely as benzene for a relative comparison.

Table 3.1: Comparison of BTEX concentrations from the *Yellow Cab* site over a 4-year period (in ppb = nmol mol^{-1}; LDL = lower detection limit).

	Max.	Mean	Median	Min.
Benzene				
Winter 2009	1.80	0.38	0.31	0.01
Winter 2012	1.94	0.36	0.29	<LDL
Spring 2013	2.48	0.31	0.22	<LDL
% Change from 2009 to 2013	38%	**-18%**	**-29%**	
Toluene				
Winter 2009	2.42	0.43	0.32	<LDL
Winter 2012	2.36	0.38	0.27	0.02
Spring 2013	3.19	0.33	0.21	0.02
% Change from 2009 to 2013	32%	**-23%**	**-34%**	
Ethylbenzene				
Winter 2009	0.30	0.06	0.05	<LDL
Winter 2012	0.60	0.06	0.04	<LDL
Spring 2013	1.66	0.06	0.04	<LDL
% Change from 2009 to 2013	453%	**0%**	**-20%**	
Xylenes				
Winter 2009	1.32	0.28	0.22	0.04
Winter 2012	1.92	0.26	0.19	<LDL
Spring 2013	3.82	0.26	0.17	0.03
% Change from 2009 to 2013	89%	**7%**	**-23%**	

In table 3.2, we compare our flux results from the spring 2013 and winter 2012 periods to the winter 2009 data from Park et al., (2010). Here we observe an even greater reduction in BTEX fluxes than concentrations with median BTEX flux reductions of 25 to 54 percent over four years, equating to an average yearly emissions drop between 7 percent for ethylbenzene and 13.5 percent for toluene between 2009 and 2013.

Table 3.2: Comparison of BTEX fluxes (in mg m^{-2} hr^{-1}) from the *Yellow Cab* site over a 4-year period (in ppb = nmol mol^{-1}; LDL = lower detection limit).

	Max.	Mean	Median	SD
Benzene				
Winter 2009	1.52	0.21	0.17	0.23
Winter 2012	1.34	0.07	0.06	
Spring 2013	2.28	0.09	0.08	0.16
4-year % Change	50%	**-57%**	**-53%**	
Toluene				
Winter 2009	4.54	0.35	0.24	0.47
Winter 2012	3.40	0.19	0.07	
Spring 2013	7.31	0.26	0.11	0.64
4-year % Change	61%	**-26%**	**-54%**	
Ethylbenzene				
Winter 2009	0.86	0.07	0.04	0.09
Winter 2012	0.84	0.03	0.02	0.12
Spring 2013	3.02	0.07	0.03	0.21
4-year % Change	251%	**0%**	**25%**	
Xylenes				
Winter 2009	4.33	0.23	0.14	0.35
Winter 2012	3.23	0.14	0.08	0.36
Spring 2013	10.85	0.23	0.10	0.66
4-year % Change	151%	**0%**	**-40%**	

It is important to note that while there are considerable variations between consecutive years, a clear overall trend of flux reductions is observed over a 4-year period. In order to explain some of the lower fluxes for the winter 2012 period, we looked at the difference in the meteorological data between the two periods. The average temperatures were 15.2 °C, 15.7 °C, and 20.7 °C for the winter 2009, winter 2012, and spring 2013 sampling periods respectively. As mentioned in Park et al. (2010), we are aware of significant evaporative emissions occurring within the study area, thus making a case for the higher emissions during the spring 2013 period as an average 5 °C temperature increase should produce greater VOC evaporation emissions. To further

pinpoint emissions sources, we broke down measured emissions by wind directions and temperature ranges as in Table 3.3 and 3.4, respectively. Benzene fluxes were larger in the spring 2013 period under similar wind directions, while xylene fluxes were comparable from similar wind directions and temperatures. Toluene fluxes were significantly higher out of southeasterly wind directions than northeasterly wind directions for both periods with very low toluene fluxes from northeasterly wind directions, especially during the winter 2012 period. This toluene flux result is expected as toluene is a major component of the primer used by Yellow Cab's paint and body shop located approximately 100 meters southeast of the tower. Toluene fluxes were similar with temperatures greater than 20 °C for both periods, while toluene fluxes were significantly less in the winter 2012 period with temperatures less than 20 °C. Ethylbenzene had similar fluxes with southeasterly wind directions and temperatures greater than 20 °C, while ethylbenzene fluxes were almost imperceptible with temperatures less than 20 °C or northeasterly wind directions during the winter 2012 period.

Table 3.3: Temperature, sample size, and median BTEX fluxes (mg m^{-2} hr^{-1}) from different wind directions during the winter 2012 and spring 2013 sampling periods.

	Winter 2012 Wd: 90 – 200	Spring 2013 Wd: 90 - 200	Winter 2012 Wd: 340 - 90	Spring 2013 Wd: 340 - 90
Sample Size (hours)	150	439	185	155
Average temperature (°C)	19.9	22.6	13.1	16.1
Benzene flux	0.063	0.087	0.041	0.049
Toluene flux	0.140	0.108	0.021	0.066
Ethylbenzene flux	0.024	0.025	0.001	0.031
Xylenes flux	0.104	0.103	0.047	0.047

Table 3.4: Sample size and median BTEX fluxes (mg m^{-2} hr^{-1}) under different temperatures for the winter 2012 and spring 2013 sampling periods.

	Winter 2012 10°C - 20°C	Spring 2013 10°C - 20°C	Winter 2012 20°C - 30°C	Spring 2013 20°C - 30°C
Sample Size (hours)	191	243	139	428
Benzene flux	0.057	0.066	0.058	0.094
Toluene flux	0.052	0.097	0.121	0.116
Ethylbenzene flux	0.006	0.031	0.026	0.031
Xylenes flux	0.700	0.072	0.106	0.116

Of interesting note, we did not observe a significant reduction in mean ethylbenzene and xylene fluxes (Table 3.2). This is largely attributable to a xylene emissions source approximately 200 m SW of the tower, as shown in figure 3.5, that creates Xylan® coatings in the manufacturing of their products (http://www.swplating.com). It is understood that commercial xylenes (80% actual m-, p-, and o-xylenes, and 20% ethylbenzene) are used as a solvent and dilution method in the production of Xylan® coatings (Badesha, 1999). Under SW wind directions, large fluxes of xylenes and ethylbenzene were observed, but because this wind direction occurred rarely during the spring 2013 period and almost never occurred during the winter 2012 period, there was little effect on the mean flux of ethylbenzene and xylenes.

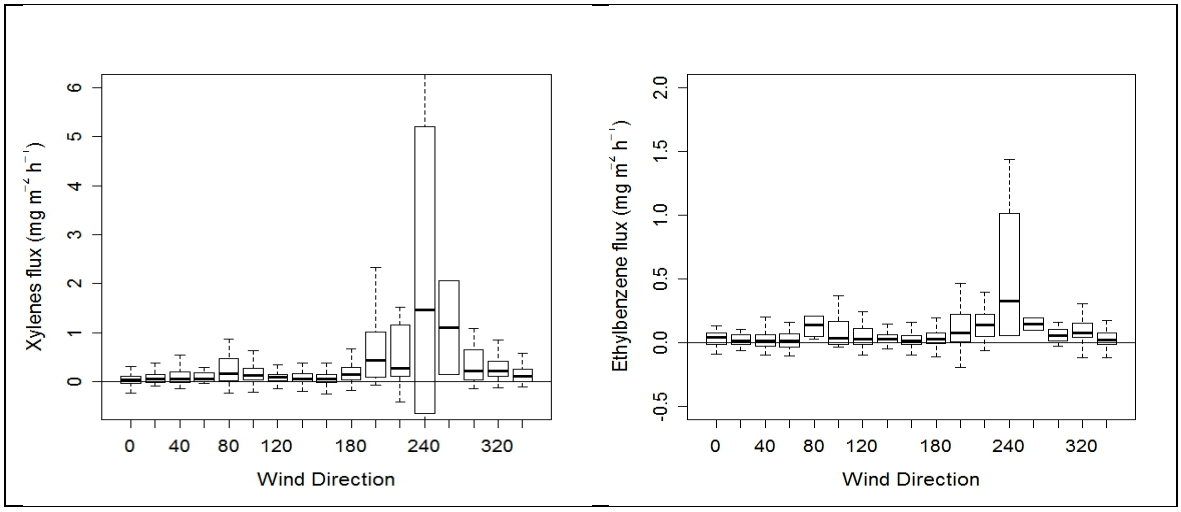

Figure 3.5: Evidence of a commercial xylenes (includes ethylbenzene) source from boxplots of the sum of o-,m-, and p-xylene flux (left) and ethylbenzene flux (right) versus wind direction during the spring 2013 period.

3.2 Comparison of Traffic Counts to Selected Vehicle Exhaust VOC Fluxes

In order to relate the VOC measurements observed at the tower to surface sources, it is important to analyze the nature of the sources at the surface within the footprint region. As mentioned in the methodology section, traffic counts were taken on major commuter roads and neighborhood streets in the study region in 2011 and 2012, and local Yellow Cab parked and idle vehicle counts were obtained in September 2013. A comparison of observed traffic counts to measured VOC fluxes was performed in order to distinguish evaporative and industrial emissions from running vehicular emissions. We compared fluxes of VOCs with minimal regional industrial point sources but that are commonly found in running vehicle exhaust from gasoline-powered engines, such as isopentane, isooctane, and benzene, with locally emitted toluene.

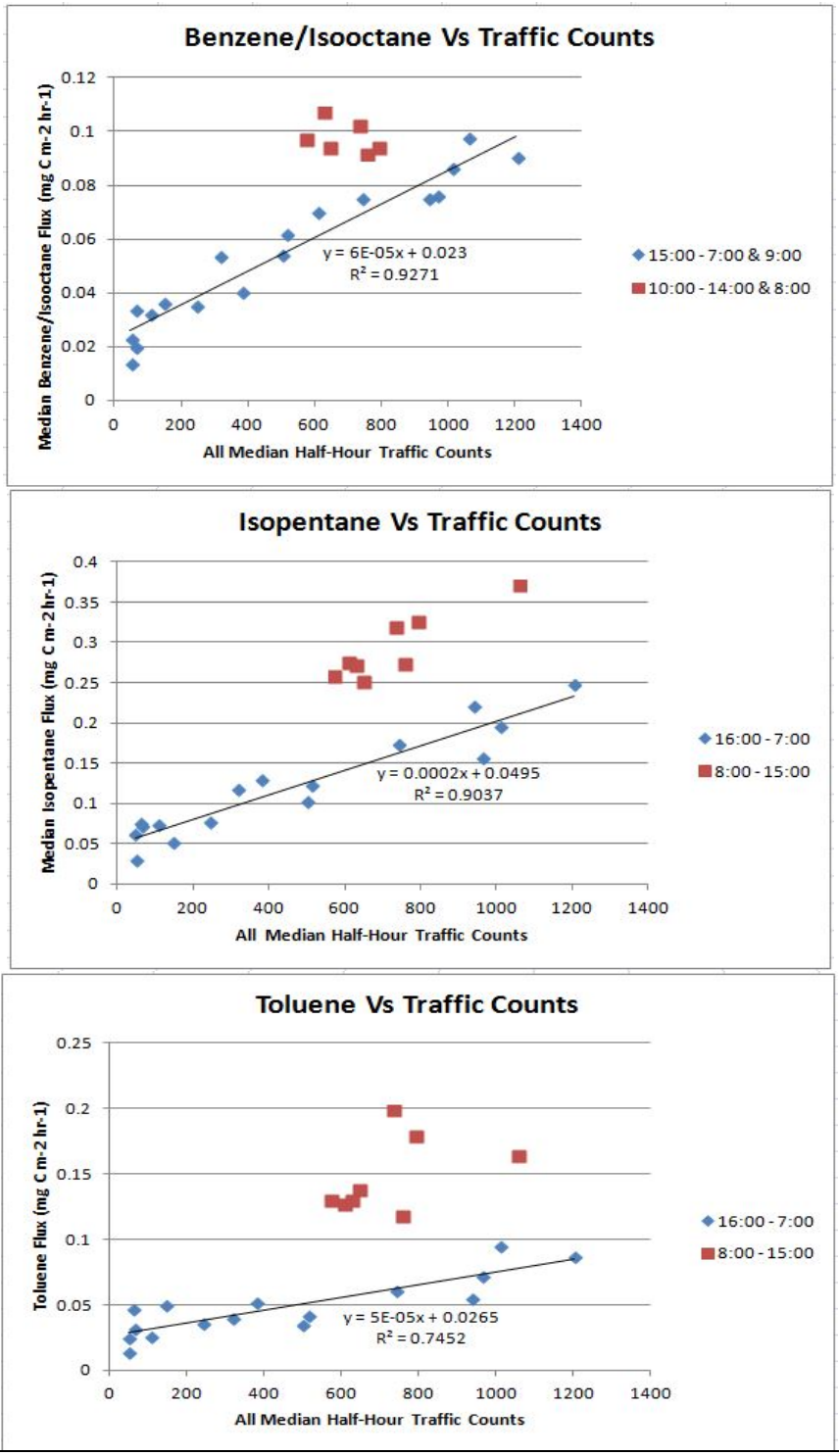

Figure 3.6: Median benzene/isooctane, isopentane and toluene fluxes (mg C m^{-2} hr^{-1}) from the spring 2013 period versus the sum of all median half-hour traffic counts (shown in figure 2.3). Red squares show variable working hours and blue diamonds show the remaining hours of the day.

Figure 3.6 shows a generally strong correlation between selected VOC fluxes during variable non-working hours and the summation of all observed daily median traffic counts from all roads shown in figure 2.3. To account for the summation of all local neighborhood streets, median Luzon traffic counts were multiplied by 10, while all other street counts were equally weighted. Determination coefficients ranged from R^2 = 0.75 for toluene to R^2 = 0.93 for isooctane/benzene. Isooctane and benzene are lumped together as these species do not separate on our chromatogram as mentioned in section 2.3.4. Additionally, isooctane was shown to be a larger component of tailpipe emissions than benzene during the Washburn tunnel measurements in Houston as a part of the 2000 Texas Air Quality Study (McGaughey et al., 2004). Benzene and isooctane have proven to be most directly related to tailpipe emissions with the strongest correlation to traffic counts and only 6 working hours that appeared to have slightly larger fluxes. Isopentane also had a strong correlation to traffic counts; however the working hours, approximately from 8:00 – 15:00, show significantly higher emissions than benzene and isooctane. This is a reasonable result, because isopentane has a much higher vapor pressure. Its daytime evaporation is thus more strongly influenced by increasing temperatures. Toluene had the lowest correlation to traffic counts and even higher working hour emissions than isopentane, suggesting it is least correlated to traffic and has other emissions sources such as its use in Yellow Cab's paint and body shop as a main constituent of their paint primer.

During most working hours, larger VOC fluxes were observed than median half-hour traffic counts would suggest. This implies that there are likely additional emissions

sources such as evaporation and/or industrial emissions. Considering there are up to 400 cars parked and 25 cars idling during the afternoon in the *Yellow Cab* parking lots on a daily basis (Figure 2.4, section 2.2) in addition to numerous industries surrounding the tower, it is safe to assume there are significant non-road VOC emissions within the flux footprint region unrelated to the local traffic counts, especially during the daytime working hours. Park et al. (2010) also came to the conclusion that evaporative emissions were significant because data obtained during the cooler winter period showed much lower evaporative emissions than were measured during their summer 2008 measurement period.

To better understand source contributions during these variable working hours, we compared correlations of our VOC fluxes to our Yellow Cab car counts, class B vehicles (large trucks) and buses from all streets, all vehicles from all streets, and specifically Loraine street, with data summarized in table 3.5. We observed the best correlations with Loraine street vehicle counts, which had the highest percentage of larger vehicles at 17 percent during the afternoon hours with an R^2 of 0.89 for benzene/isooctane. We also observed higher correlations for all three VOCs when considering only *large* vehicle counts versus *all* vehicle counts. This would suggest that larger vehicles such as trucks and buses have a larger emissions impact than regular passenger vehicles. Additionally, we found good correlations between the Yellow Cab parked car counts, especially for toluene with an $R^2 = 0.67$ correlation, suggesting there are significant vehicle evaporative emissions from parked cars directly surrounding the tower. Using a multi-linear regression, all of these factors were significant at the 95%

level, suggesting all factors have a contribution to the measured net VOC emissions. Although strong multilinear regressions were observed using the five correlations listed in Table 3.5, these correlations were not conclusive enough to dismiss working-hour industrial emissions as a contributor to our measured VOC emissions, for example because parked car counts co-vary with the local paint shop emissions as both are work-hour related. Unfortunately, an activity schedule of the local paint shop could not be obtained, and therefore a significant fraction of net emissions remained unexplained other than through the parked car working-hour proxy (Table 3.5).

Table 3.5: R^2 correlations between benzene/isooctane, isopentane and toluene fluxes and other observed daily counts.

	Benzene/Isooctane	Isopentane	Toluene
YC Car Counts (7:15 – 19:15)	0.57	0.43	0.67
YC Idling Car Counts (7:15 – 19:15)	0.12	0.20	0.23
All Large Vehicle Traffic Counts (all hours)	0.78	0.76	0.52
All Vehicle Traffic Counts (all hours)	0.72	0.62	0.38
Loraine St Traffic Counts (all hours)	0.89	0.74	0.57
Multilinear Regression R^2	0.97	0.96	0.93

3.3 Verification of a Bulk Footprint Model Using VOC Tracer Releases

The bulk flux footprint model of Kormann and Meixner (Kormann and Meixner, 2001) as part of the EdiRe flux analysis software (University of Edinburgh, UK) used in

our data processing stages was introduced to test its validity in an urban heterogeneous environment to assign measured bulk fluxes to local sources. The Kormann and Meixner model assumes a homogenous underlying surface and well-defined atmospheric turbulence regimes. The model uses input parameters of measurement height, wind speed, wind direction, friction velocity, Monin-Ohbukov stability (z/L), and the standard deviation of the crosswind variation. These few bulk input parameters provide an ease of use and comparatively simple footprint computation with satisfactory correspondence under unstable and neutral conditions to a more sophisticated Lagrangian model, which require greater computational resources and time (Kljun et al., 2004, Kljun et al., 2003, Kljun et al., 2002). Generally, the model output is a map of source probability density (the footprint function), which in this case was chosen to be a 30 m x 30 m square grid map out to 3 km distance from the tower. At the Yellow Cab site, the surface layer turbulence is consistent with previous urban measurements (Roth, 2000), and our measurement height of 60 m is approximately six to ten times the displacement height and therefore very likely well outside the roughness sublayer. Thus, the chosen footprint model output should represent a qualitatively correct picture of surface area contribution, albeit at the displacement height. However, this model has not been rigorously tested in a more turbulent and complex heterogeneous urban environment with a substantial roughness sublayer expected to affect pollutant dispersion.

To test the model's accuracy in this environment, we released known quantities of acetone and methyl-ethyl-ketone (MEK) in upwind locations within the footprint of the tower during the half-hour sampling period of the GC, using either hand-pressurized

pump sprayers to create a fine mist or evaporating the VOC's from a warm concrete surface using an electric leaf blower. Thus, the known amount of VOC emitted multiplied by the average contribution of the 30 m x30 m grid points where the release occurred was compared to the flux measured at the GC. Error estimates were included for both the measured net flux and the released VOC amounts.

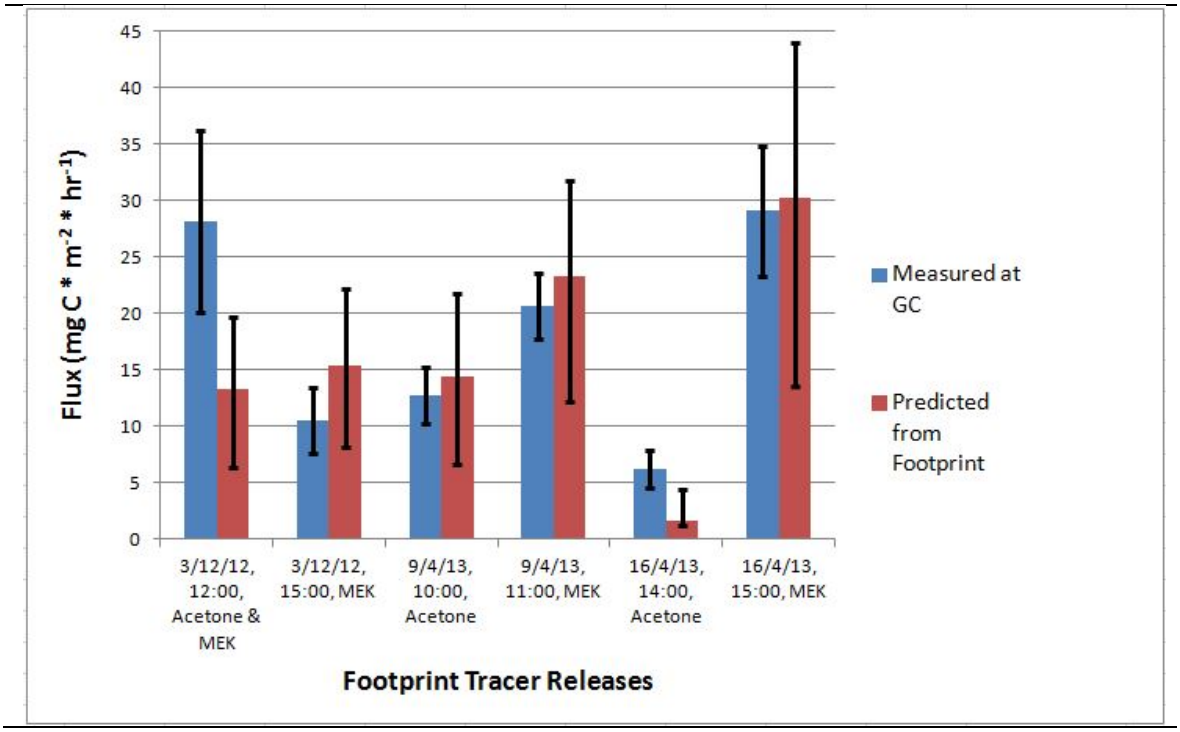

Figure 3.7: GC measured fluxes versus footprint-predicted fluxes of 6 separate tracer releases with error bars calculated from equation 3.1 and 3.2 for the GC measured and footprint predicted fluxes, respectively.

Figure 3.7 shows a summary of the 6 tracer releases performed for this validation study of the Kormann and Meixner footprint model, including the calculated error bars for both the REA-GC system and the footprint model (discussed below). For the REA

GC system measured fluxes, Kota et al. (2014) described the absolute analytical uncertainty ($u_{i,j}$) through an error propagation of the up and downdraft concentration and vertical wind speed uncertainties as follows:

$$u_{ij} = \sqrt{\left(\frac{\Delta C}{C}\right)^2 \frac{C_{up,i,j}^2 + C_{down,i,j}^2)}{\left(C_{up,i,j} - C_{down,i,j}\right)^2} + \left(\frac{\Delta \sigma_w}{\sigma_w}\right)^2} \quad (3.1)$$

where the relative uncertainty of concentration (□C/C) in up and downdrafts was taken as 10 percent and the relative uncertainty of σ_w (□σ_w/ σ_w) was taken as 5 percent. These set uncertainties are based upon investigations done by Park et al. (2010) using the same set up.

Footprint model uncertainties are unspecified, and we thus developed reasonable error estimates by assuming that the input variables to the footprint model are only known to various degrees of accuracy, respectively vary with height above the surface – as opposed to staying constant throughout the surface layer as assumed by the model – due to canopy and roughness layer influences. We varied the Monin-Ohbukov stability factor (z/L), the friction velocity (u*) and the standard deviation of crosswind variation (sd.v) by up to 20%, and chose the regular 7 meter displacement height (d) to vary by up to 3 meters. We ran the footprint model with each of these errors in place separately and compared the varied average footprint contribution to the base average footprint contribution of the grid points where the tracer releases occurred. The absolute uncertainty (u) of the footprint output due to these variables was propagated as follows:

$$u = \sqrt{\left(\frac{\Delta(\frac{z}{L})}{z/L}\right)^2 + \left(\frac{\Delta u*}{u*}\right)^2 + \left(\frac{\Delta(sd.v)}{sd.v}\right)^2 + \left(\frac{\Delta d}{d}\right)^2} \quad (3.2)$$

As can be seen in Figure 3.7, four out of six releases were in good agreement, with the remaining two releases a factor of 2-3 apart, but almost within the combined calculated levels of uncertainty. The 12:00 and 15:00 h releases on December 3rd had the largest release areas of 29,700 m^2 (33 grid points) while the largest area of the other four releases was only 5,400 m^2(6 grid points). The large absolute discrepancy in the 12:00 h release on 3 December can be attributed to the GC receiving a disproportionally larger percentage of the VOCs released within higher contribution grids, as there was approximately a factor of 10 difference between individual grid contributions in the release area during that half hour. The discrepancy of the 14:00 h release on April 16th may have been caused by a large variation in individual grid contributions during the 30-min release as the release area was on the edge of a sharp footprint contribution gradient, depicted in Figure 3.8. For comparison, Figure 3.8 includes the April 16th 15:00 h release, for which we observed almost identical calculated and measured fluxes but which occurred in the 'bulls eye' of the footprint function surrounded by near uniform grid contributions.

16/4/13 14:00 CDT, Acetone release

16/4/13 15:00 CDT, MEK release

Figure 3.8: Tracer releases from April 16th, 2013. The red shaded areas show higher footprint impact areas. The light yellow to grey shaded areas have little to no footprint impact. The 14:00 release occurred on the edge of a strong footprint contribution gradient whereas the 15:00 release occurred in a uniformly high-contribution area.

Large differences between measured and predicted surface source impacts can occur based on non-linear averaging, such as receiving a larger updraft that is sampled from the source area during small turbulent fluctuations not balanced by similar sampling periods during updrafts not from the source area. Our tracer release results suggest that this most likely occurs when the release area is located towards the edge of the (average 30-min) footprint function or in areas where a strong horizontal flux contribution gradient exists.

3.4 Verification of a Bulk Footprint Model Using a Known n-pentane Source

There are multiple buildings that belong to Houston Foam Plastics (HFP), a company known to emit n-pentane as part of their foam storage and production processes, located between 1.2 km and 2.0 km SSE of the Yellowcab tower. The facility fabricates polyethylene, polypropylene, and polystyrene foam plastics (http://www.houstonfoam.com). These foams are produced using n-pentane as blowing agent, which forms bubbles to expand and mold the foam to a desired shape (Grimminger and Muha, 1995). As it is a large facility with over $100 million in yearly revenue (http://www.insideview.com/directory/houston-foam-pastics-inc), HFP has large production volumes and thus significant emissions that require them to have a Texas Commission on Environmental Quality (TCEQ) air permit to operate (TCEQ permit 19940). Their permit allows for a maximum emission rate of 23.08 pounds per hour (10.5 kg per hour) and a maximum yearly emission of 45.24 tons per year corresponding

to a 10.33 pounds per hour (4.67 kg per hour) yearly average. Also listed in the company's permit are the allocated sources for these VOC emissions, of which over 99.5% belong to evaporative emissions from box opening, molding, and block storage solely attributable to the n-pentane that comes packaged within the unmolded foam (Grimminger and Muha, 1995).

Emissions of n-pentane from the HFP facility are obvious when plotting measured n-pentane mixing ratios and net n-pentane fluxes against wind direction, shown in Figure 3.9. Clear peaks occur for wind directions directly from the facility. Large fluxes of n-pentane were first discovered at this site by Park et al. (2010) in the summer of 2008. At the time, these emissions were assumed to be sourced from car traffic. The winter 2012 period only had 14 useable half-hour flux measurements from wind directions in the 145-185 degree sector, but out of the 690 half-hour measurements during the spring 2013 period, 146 were useable and from wind directions between 145° - 185°.

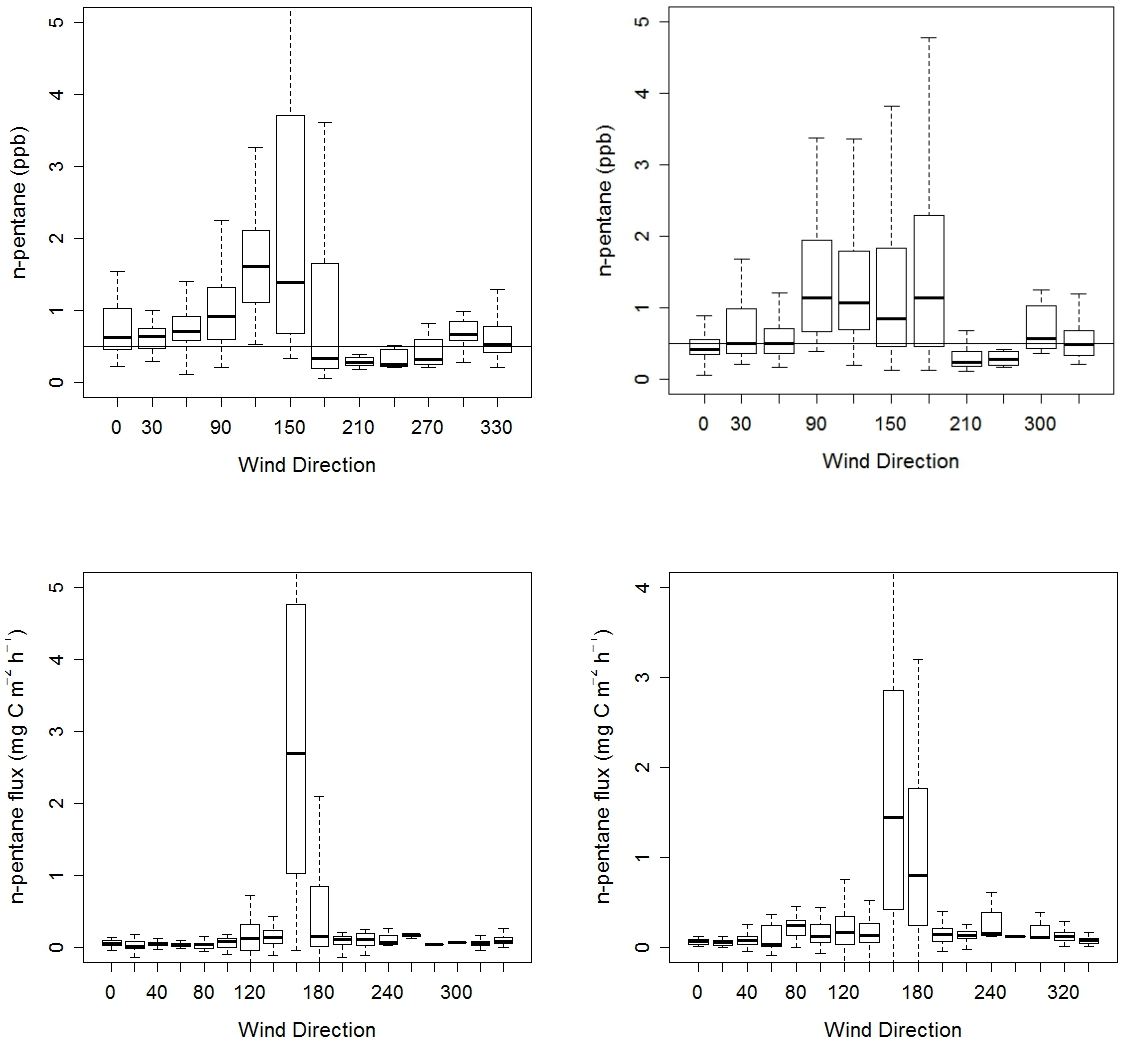

Figure 3.9: Evidence of an n-pentane source from boxplots of n-pentane concentration (top) and n-pentane flux (bottom) versus wind direction from the winter 2012 period (left) and the spring 2013 period (right).

To ensure the pentane fluxes considered were solely from the facility, a background of n-pentane flux was subtracted using our observed flux ratio of 1.4:1 isopentane/pentane from non-185° - 145° directions, thus excluding biased wind directions from the source containing high pentane emissions. This isopentane/pentane

ratio is shown in Figure 3.10 in which all graphs show a molar isopentane/pentane ratio of 1.4:1 except for the winter 2012 period during which a slightly higher ratio at 1.6:1 was observed. The 1.4:1 ratio is identical to the ambient concentration ratio of 1.39:1 measured in Houston during the 2006 TexasAQS as reported by Gilman et al. (2013), but is significantly lower than found in most other US cities, which nearly all had ratios between 2:1 and 3:1 of isopentane/n-pentane in the past (Baker et al., (2008). For comparison, we evaluated a gasoline sample from a local gas station in Houston in November of 2013 and tested its liquid and headspace composition in the laboratory, discovering an isopentane/n-pentane ratio of 1.23 and 1.48, respectively.

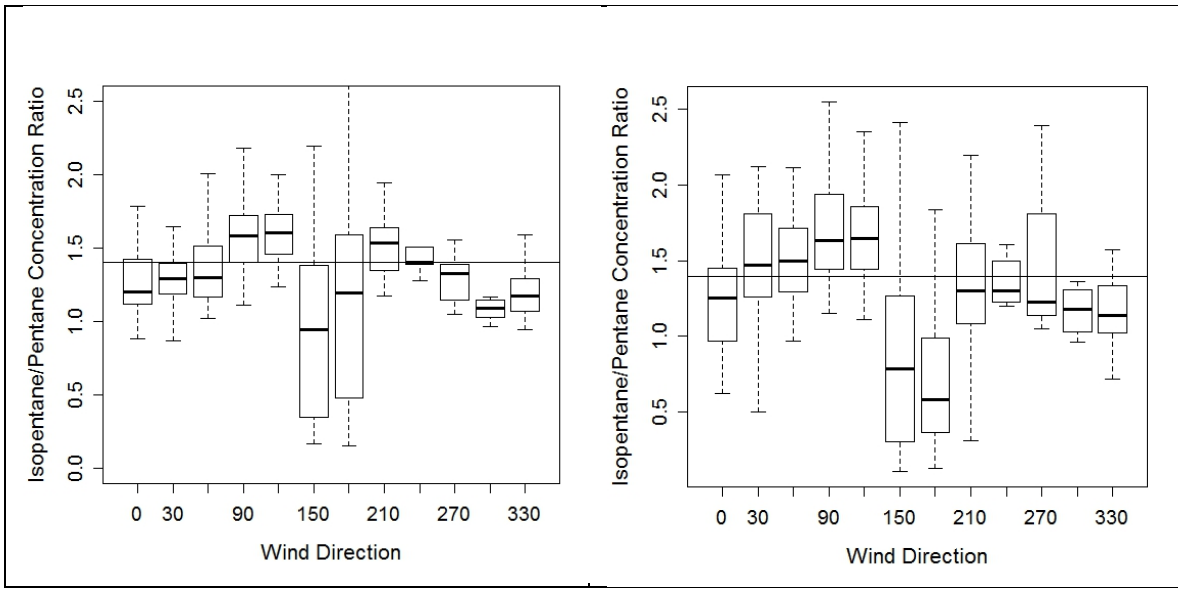

Figure 3.10: Isopentane/n-pentane concentration (top) and flux (bottom) ratios from the winter 2012 (left) and spring 2013 (right) periods. The line in the flux ratio from winter 2012 is 1.6:1 while the other lines are 1.4:1.

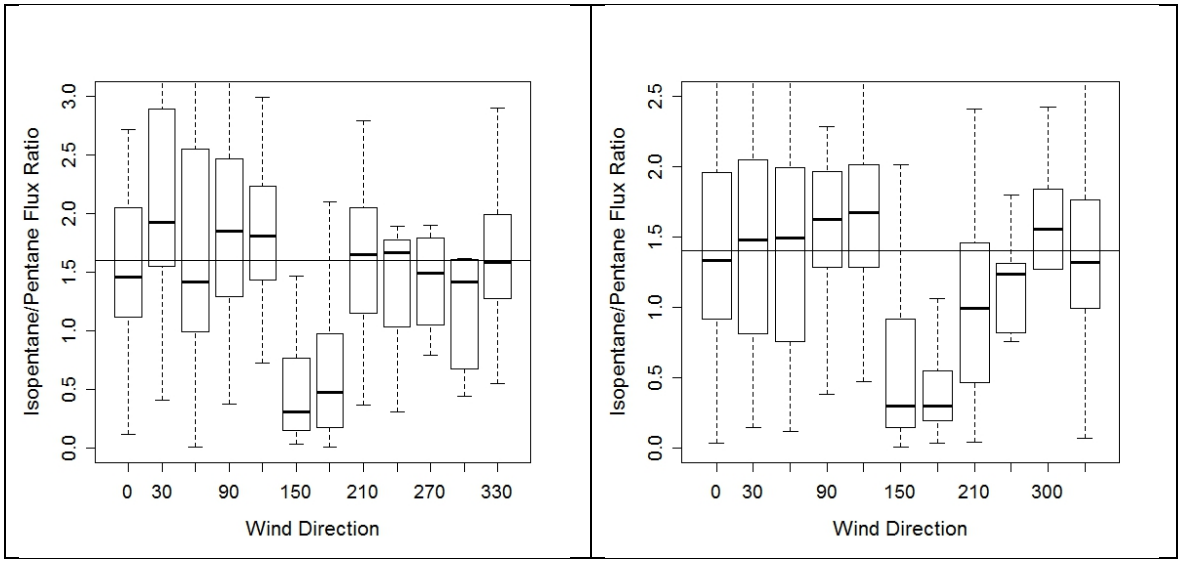

Figure 3.10 Continued.

We applied the Kormann and Meixner footprint model to estimate the n-pentane flux from the buildings owned by HFP. Under SSE winds, this facility falls within a moderate to low contribution area of the footprint function with individual 30 m x30 m grid points each containing roughly a 10^{-4} share to the total flux (Figure 3.11), which is approximately ten times less than the grid points evaluated for the tracer release experiments. While the tracer releases were emitted within areas with the strongest footprint contributions a few hundred meters from the tower, the HFP buildings are located at a much larger distance away and may thus be a good test of the accuracy of the footprint model at distance (Figure 3.11).

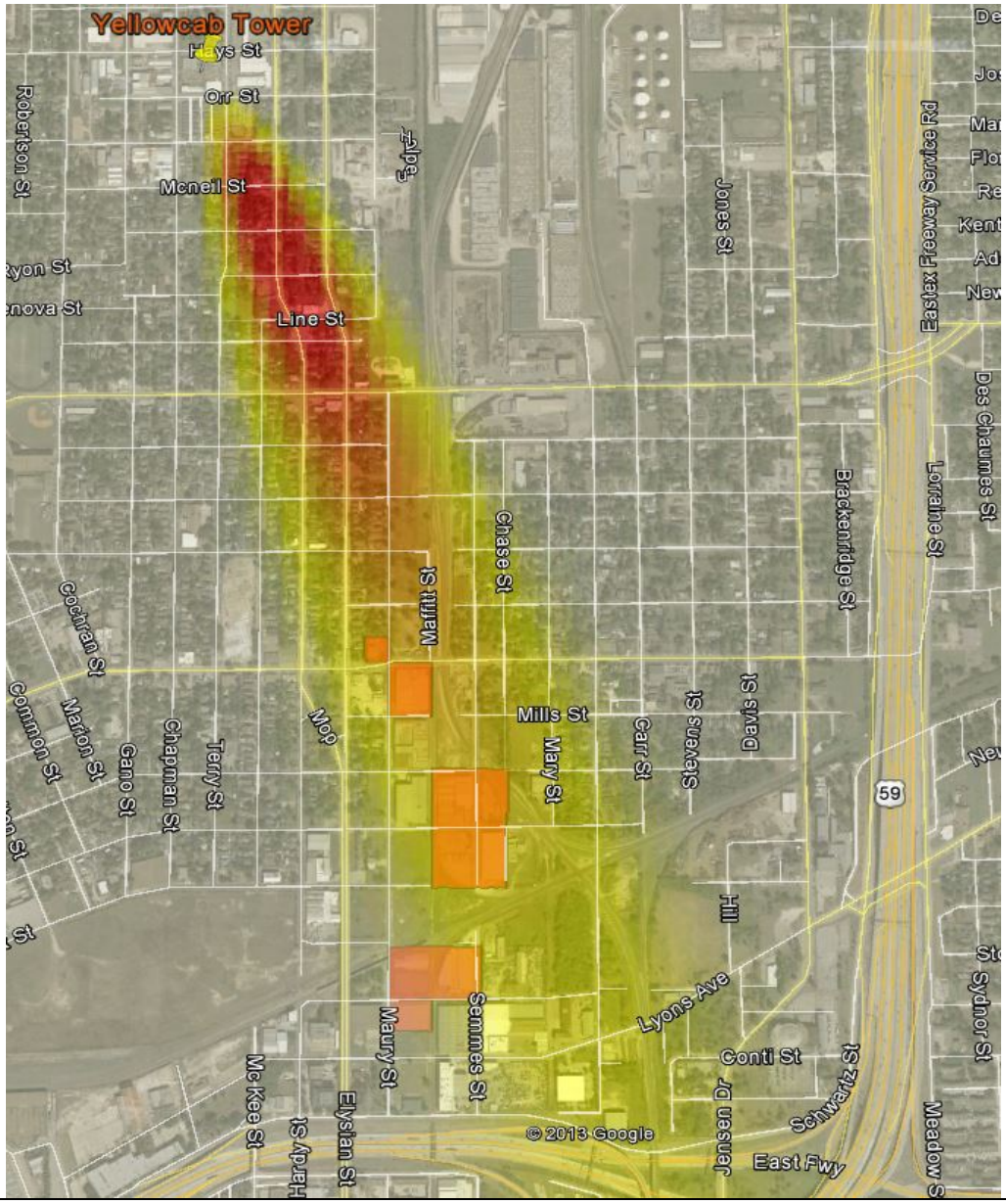

Figure 3.11: Sample flux footprint for a SSE wind direction. Highlighted in orange are buildings that belong to Houston Foam Plastics. Here, most of the facility falls into a zone where 30 m x30 m grid points contain roughly 1 to 5 x 10^{-4} total footprint contributions. All grids highlighted in orange were averaged together for emissions calculations.

HFP's emissions were calculated by dividing the n-pentane flux measured at the tower by the average 30 m x30 m grid footprint contribution of the facility as outlined in equation 3.3:

$$HFP\ Emission\ (\frac{lbs}{hr}) = \frac{\left(n-pentane - \frac{5}{7}isopentane\right)Flux\left(\frac{\cancel{mg}}{\cancel{m^2}hr^1}\right)\left(\frac{1\ lb}{4.536*10^5\ \cancel{mg}}\right)(900\cancel{m^2})}{Average\ 30x30m\ grid\ contribution} \quad (3.3)$$

For the emissions rate analysis, individual periods were omitted from the analysis if the domain sum of the flux probability was less than 0.7 to ensure that a sufficient amount of the total flux footprint lay within the computational domain. For example, there were 44 hours measured by the GC with wind directions between 145° - 185° in the winter 2012 period, but only 14 of those hours had a domain sum of the flux probability greater than 0.7.

While many individual emission calculations show the facility is operating well above their TCEQ air permit, the calculated emissions with wind directions in line directly from the facility's buildings between 158° - 169° show a median and average n-pentane emission of 11.6 lbs/h and 14.0±8.0 (1 sd) lbs/h, respectively, Figure 3.12. We think these are accurately calculated emissions as they fall within the company's permitted emissions rate of 23.08 lbs/hr, but are outside of their average yearly rate of 10.33 lbs/hr. Importantly, these emission calculations are significantly lower than those made by Kota et al. (2014) who calculated a median emission rate of 34.6±6.8 lbs/hr, using the July 2008 data from Park et al. (2010) and a Monte Carlo technique. However, Kota et al. (2014) (i) presumed an assigned emissions composition that included other VOCs aside from n-pentane based on an EPA emissions

profile, and (ii) did not directly subtract background n-pentane fluxes using the empirical isopentane ratio developed for this site.

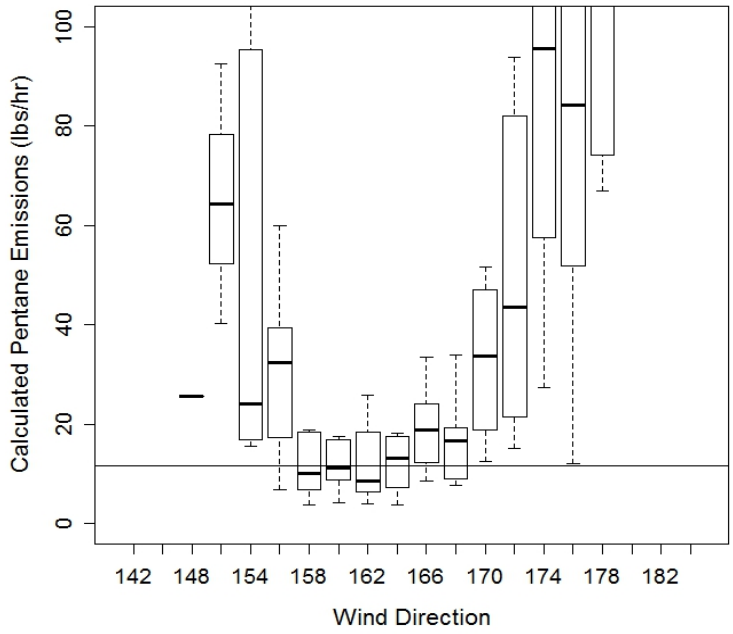

Figure 3.12: Boxplot of calculated HFP n-pentane emissions versus wind direction. Horizontal line shows the median emission of 11.6 lbs/h for wind directions directly from HFP between 158° - 169°.

Figure 3.13 shows a good parabolic correlation between the wind direction and HFP n-pentane emissions with a minimum of 8.76 lbs/hr at a 162° wind direction from the tower. We attempted to further investigate this relationship with other micrometeorological measurements observed from the tower such as the horizontal cross wind standard deviation, skewness, and kurtosis to see if an uneven distribution of sampling would cause a bias in underestimating the footprint area of the HFP buildings. However there were no conclusive correlations of these micrometeorological

measurements to the observed parabolic ratio of HFP emissions to wind direction as correlations were limited by usable data.

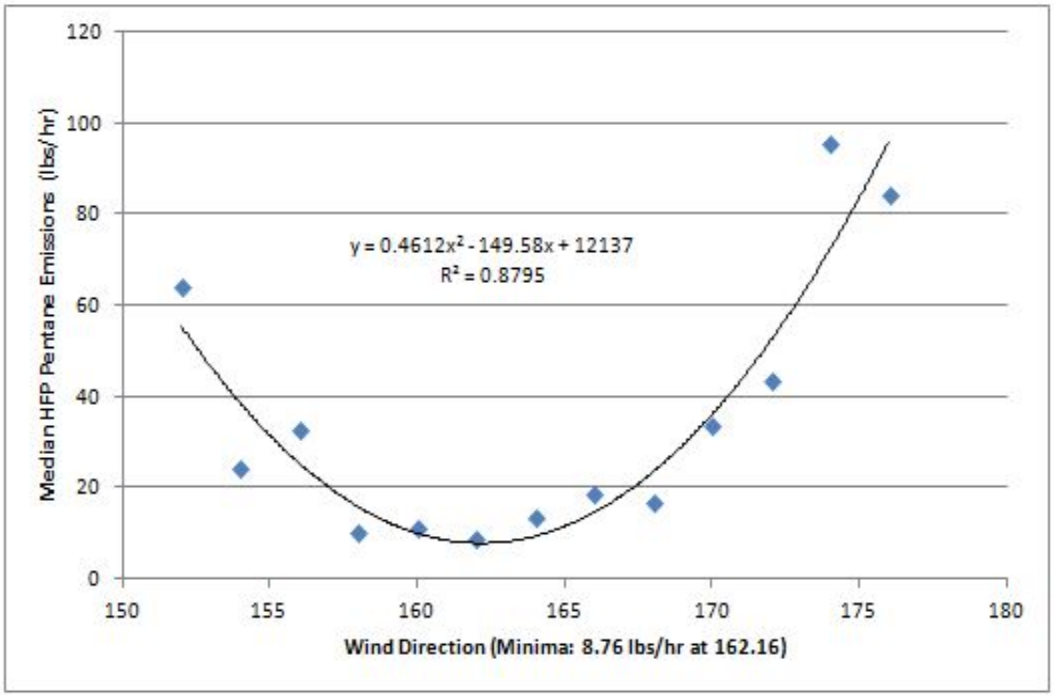

Figure 3.13: Graph of median HFP pentane emissions per 2° wind direction. The parabolic line on the graph shows an emission's minima of 8.76 lbs/h of n-pentane with a good correlation of $R^2 = 0.880$.

Since we were unable to perform an error analysis of emissions outside of wind directions directly from the facility, we focused our investigations on wind directions from 155° - 175° from the spring 2013 period, presuming that emissions calculated under these wind directions are more realistic and reliable. Similar to section 3.3, we altered the Monin-Ohbukov stability parameter (z/L), friction velocity (u*), displacement height (D), and standard deviation of the horizontal cross wind (sd.v) components of the footprint model to see how this affects HFP n-pentane emissions

calculations under stable (z/L > 0.5), neutral (0.5 > z/L > -0.5), unstable (-0.5 > z/L > -3), and very unstable (z/L < -3) atmospheric turbulence conditions. This study's sample size was 42 half-hour measurements in which 9 were classified as very unstable conditions, 21 were unstable, 8 were neutral, and 5 were stable. Table 3.6 summarizes this evaluation showing that D minimally changed the calculated HFP pentane emissions under all atmospheric turbulence conditions (up to only 2.4% in the very unstable case), while larger variations occurred up to 10.3% with a 20% increase in sd.v under stable atmospheric conditions and variations up to 6.1% for a 20% adjustment in (z/L) in very unstable atmospheric conditions. The most influential variable, however, was the friction velocity (u*), with the largest variations up to 29.24% under very unstable atmospheric conditions for a 20% adjustment.

Table 3.6: Percent change in calculated n-pentane emissions from varying footprint model input parameters of displacement height (d), Monin-Ohbukov stability (z/L), standard deviation of the vertical cross wind (sd.v), and friction velocity (u*) with variable atmospheric turbulence conditions.

	Percent change in HFP n-pentane Emission calculation			
	Very Unstable (-0.5 > z/L > -3)	Unstable (-0.5 > z/L > -3)	Neutral (0.5 > z/L > -0.5)	Stable (z/L > 0.5)
9m displacement height	-1.10%	-0.18%	-0.08%	-0.17%
11m displacement height	-2.36%	-0.8%	-0.05%	-0.09%
sd.v*0.8	-.051%	-0.86%	-6.27%	-8.22%
sd.v*0.9	0.40%	-1.56%	-3.50%	-1.29%
sd.v*1.1	2.51%	2.57%	3.76%	4.72%
sd.v*1.2	5.98%	6.17%	8.40%	10.34%
(z/L)*0.8	-5.93%	-0.21%	0.03%	-0.58%
(z/L)*0.9	-2.97%	-0.23%	-0.04%	-0.32%

Table 3.6 Continued.

(z/L)*1.1	3.08%	0.06%	-0.17%	-0.09%
(z/L)*1.2	6.13%	0.34%	-0.22%	0.25%
(u*)*0.8	-19.14%	-7.51%	-2.27%	9.34%
(u*)*0.9	-10.69%	-5.07%	-2.20%	3.17%
(u*)*1.1	13.22%	6.96%	3.48%	-1.42%
(u*)*1.2	29.24%	16.16%	20.02%	-1.35%

Figure 3.14 depicts stronger effects on HFP calculated emissions with reductions to the sd.v parameter with an increasingly stable atmosphere. An increasing emission trend is observed with increases to the sd.v parameter at all stabilities. This trend is logical because stable conditions tend to have a wider footprint function, lowering the local footprint contribution, but forcing the footprint function "cone" into a narrower zone via a reduction in sd.v that instead places the facility in a higher footprint contribution area thus lowering calculated emissions (eq. 3.3). Large variations occurred with adjustments up to 20 percent to the z/L parameter only when atmospheric conditions were very unstable, as more stable atmospheric conditions would be less affected by the z/L parameter. In very unstable conditions, reductions to the z/L parameter decrease calculated emissions while increases to the z/L parameter increase calculated emissions. This trend is also logical because an increase in instability means greater boundary-layer atmospheric lift and stronger heat fluxes, thus skewing the footprint contribution area closer to the tower while reducing the contribution of the HFP grid cells further out from the tower.

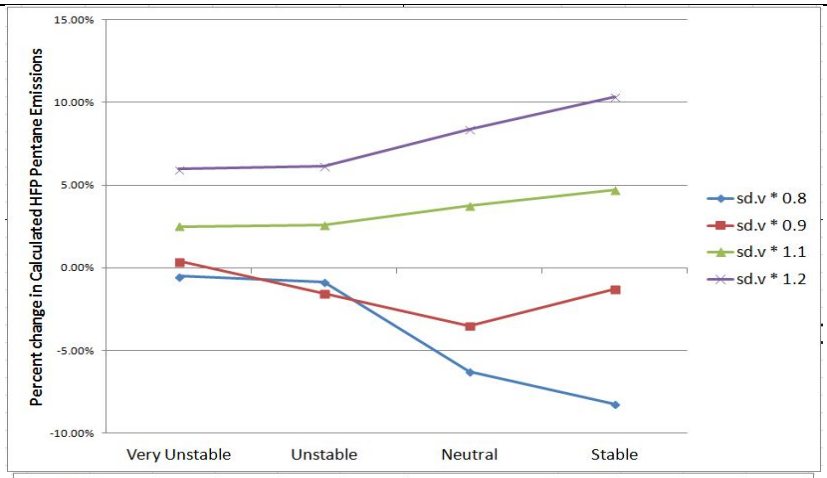

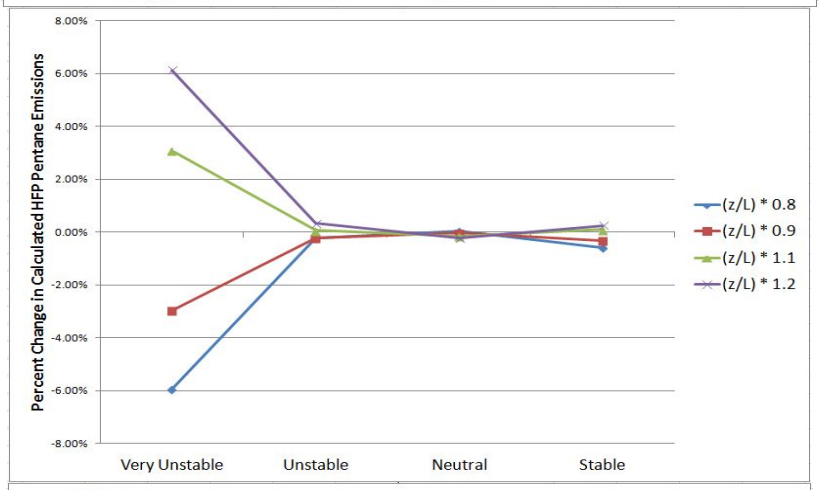

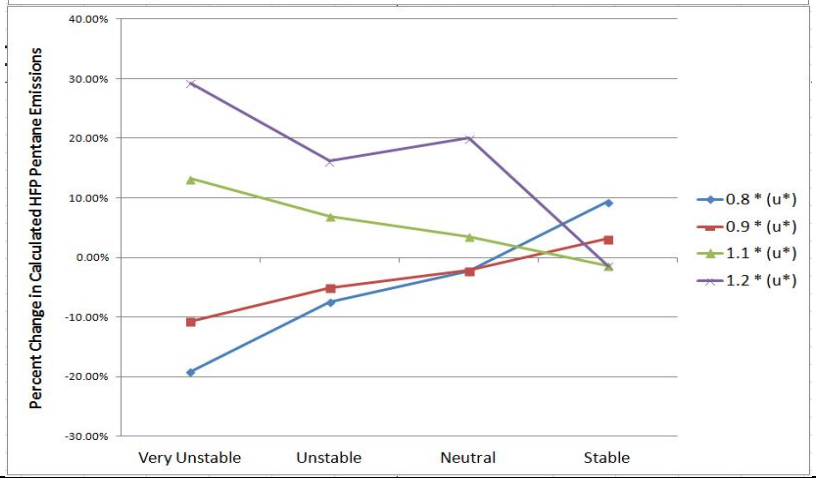

Figure 3.14: Graph of percent changes in calculated HFP n-pentane emissions by varying the standard deviation of the horizontal cross wind (sd.v), Monin-Ohbukov stability (z/L), and friction velocity (u*) model input parameters under different atmospheric turbulence conditions.

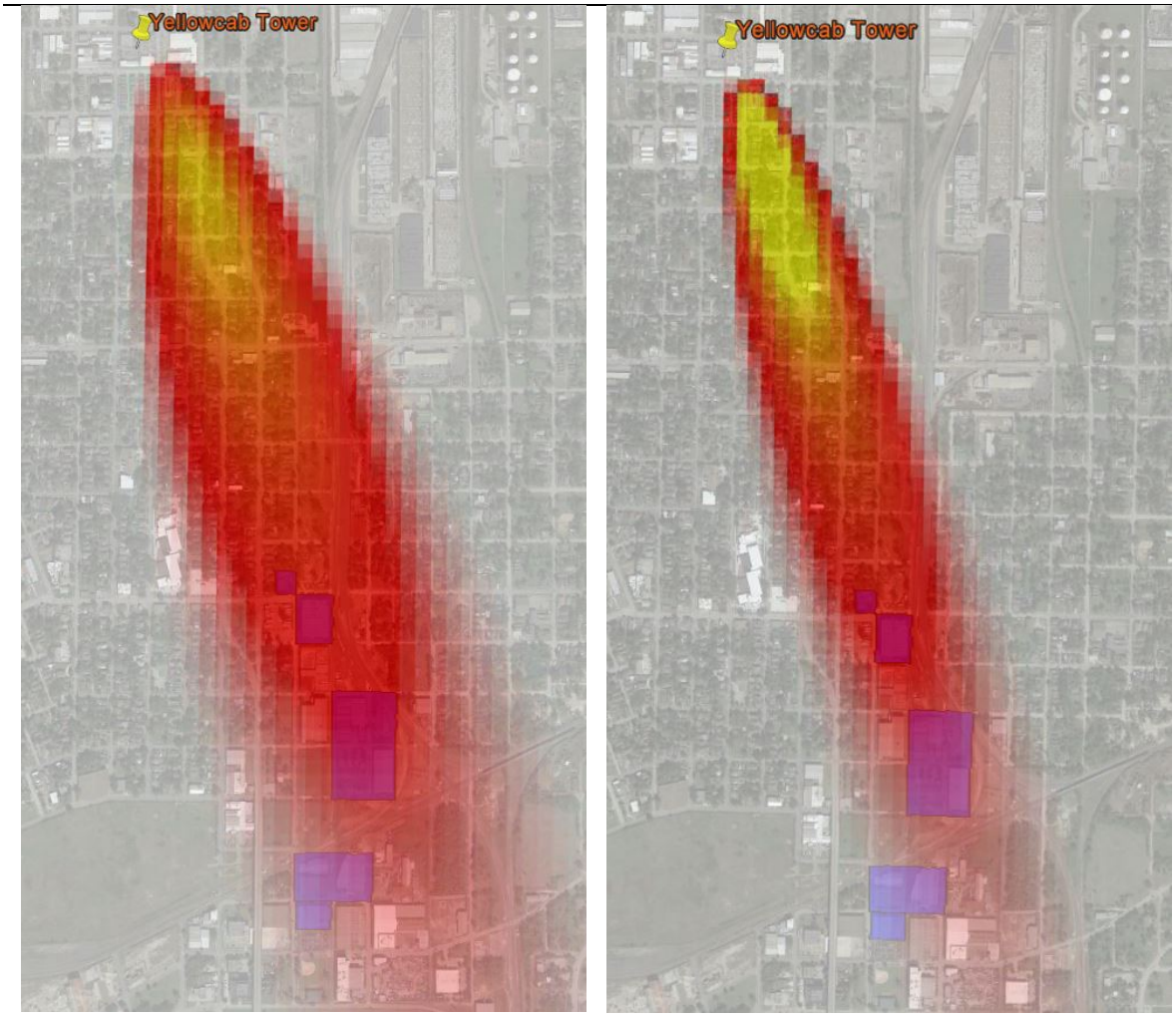

Figure 3.15: A comparison of a flux footprint model output with a 20% decrease in u* (a) versus a 20% increase in u* (b) taken from 16:00 – 16:30 CDT on March 29, 2013 under very unstable atmospheric turbulence conditions. Yellow colors show the highest impact grid points with an order of magnitude difference between yellow and red grids. Highlighted in purple are the HFP buildings.

Varying the u* parameter produced the largest differences in calculated emissions, especially in unstable and very unstable conditions. An increasing trend was observed in HFP calculated emissions with increases to the u* parameter with an increasingly unstable atmosphere, while a decreasing emission trend was observed with

decreases to the u* parameter with an increasingly unstable atmosphere. Similar to the results from adjustments to the z/L parameter, this trend is logical since larger u* values indicate an increase in turbulence, skewing the footprint contribution area closer to the tower while reducing the contribution of the HFP grid cells further out from the tower. This is depicted for an example footprint function in Figure 3.15.

4. SUMMARY AND CONCLUSIONS

In this study, we presented VOC flux measurements from a tall tower setup in a diverse urban land use region, approximately 3 km north of downtown Houston, Texas. Despite the importance of a comprehensive understanding of VOC fluxes in urban areas due to their direct and indirect effects on public health, direct flux measurements have rarely been executed because of the physically complicated urban structure, mix of emission sources, and a lack of suitable and accessible measurement platforms. Our tower setup combined with an REA GC-FID method for VOCs has allowed us to measure long term concentrations and fluxes of EPA criteria and hazardous air pollutants in an urban area.

The meteorological and geographical features of our site and the performance and quality of our system were introduced. The diurnal variations of concentration, fluxes, and traffic counts were presented with the selected BTEX measurement results during the winter 2012 period (December 5 -11, 2011, February 2 – 17 and February 22 – March 4, 2012) and the spring 2013 period (March 11 – April 20, 2013) exhibiting diurnal cycles with a dominant morning peak associated to morning rush-hour traffic. The mean and median mixing ratios during the winter 2012 period were 0.36 ppb and 0.29 ppb for benzene; 0.38 ppb and 0.27 ppb for toluene; 0.06 ppb and 0.05 ppb for ethylbenzene; and 0.28 ppb and 0.22 ppb for xylenes, respectively. The mean and median mixing ratios during the spring 2013 period was 0.31 ppb and 0.22 ppb for benzene; 0.33 ppb and 0.21 ppb for toluene; 0.06 and 0.04 for ethylbenzene; and 0.26

and 0.17 for xylenes. VOC mixing ratios agreed well with previous studies in Houston in terms of clear diurnal variations from boundary layer height and emission source dynamics. VOC flux measurements showed early morning minima in addition to a modest morning rush hour peak, but also very significant excess emissions during the afternoon hours most likely from evaporative sources. The mean and median fluxes during the spring 2013 period were 0.09 mg m^{-2} hr^{-1} and 0.08 mg m^{-2} hr^{-1} for benzene; 0.26 mg m^{-2} hr^{-1} and 0.11 mg m^{-2} hr^{-1} for toluene; 0.07 mg m^{-2} hr^{-1} and 0.03 mg m^{-2} hr^{-1} for ethylbenzene; and 0.23 mg m^{-2} hr^{-1} and 0.10 mg m^{-2} hr^{-1} for xylenes, respectively.

We noticed significant reductions in BTEX species concentrations and fluxes over a 4-year period of measurements (2009-2013), similar to recent findings analyzing other long-term measurement studies. Mean and median concentrations over the four year period fell 18% and 29% for benzene; 23% and 34% for toluene; 0% and 20% for ethylbenzene; and 7% and 23% for xylenes, respectively. Median and mean BTEX fluxes showed greater reductions than their VOC concentrations with mean and median VOC flux reductions of 57% and 53% for benzene; 26% and 54% for toluene; 0% and 25% for ethylbenzene; and 0% and 40% for xylenes, respectively.

The comparison of traffic counts to selected tailpipe VOCs showed a good correlation between traffic counts and measured fluxes, except during variable working hours. This discrepancy during working hours is most likely attributed to evaporation, larger vehicles with greater emissions than the average passenger vehicle, and point-sources, including industrial emissions.

The bulk flux footprint model of Kormann and Meixner (2001) was tested and applied to our VOC measurements. Six separate tracer releases of known quantities of acetone and MEK were carried out within the footprint region to test the accuracy of the model under urban turbulence conditions. Four out of six tracer release experiments were in surprisingly close agreement, while the other two release experiments showed larger discrepancies just outside the combined error estimates; this, however, could be explained, and was further supported by our second test of the footprint reliability. These releases verified that the footprint model works surprisingly well within close proximity to the receptor and when considering mostly the main impact region.

A more comprehensive test of the footprint model was performed using emissions from a foam plastics manufacturing facility. Using measured GC fluxes and footprints with wind directions directly from the facility while limiting the domain sum of the flux probability to greater than 0.7, we were able to calculate the facility's emissions. Wind directions in line directly from the facility's buildings between 158° - 169° show a median and average n-pentane emission of 11.6 lbs/h and 14.0±8.0 (1 sd) lbs/h, respectively. These rates fell within the facility's TCEQ permitted hourly emissions allowing 10.5 kg of VOC per hour. However, if occurring daily, the calculated emission would be above the permit's yearly emission rate of 4.67 kg of VOC per hour at a 68% likelihood based on a normal distribution. Varying the footprint model input parameters by up to 20% did affect the outcome of the emission calculation up to 29.2%, but these variations are relatively small compared to the natural emission variation. The footprint model did not perform well when wind directions were significantly off the

direct line from the facility (158° - 169°), but further analysis did not confirm any correlations to this discrepancy. However, implementing this footprint model with measured fluxes from our tower set up was very successful in establishing an accurate estimate of the facility's emissions under direct line winds, assuming the company is in compliance with its air permit and all HFP buildings had equal emissions. This is the first known study to test this model on a real-world industrial emissions source. Further studies are needed to verify our results, as a similar set up would be a relatively easy and non-invasive method for government agencies and private companies to calculate real-world emissions from permitted industrial activities.

REFERENCES

Ackman, R.G., 1964. Fundamental groups in the response of flame ionization detectors to oxygenated alphatic hydrocarbons. *J. Gas Chrom.*, 2(6): 173-179.

Ackman, R.G., 1968. Flame ionization detector – further comments on molecular breakdown and fundamental group responses. *J. Gas Chrom.*, 6(10): 497-501.

Ammann, C. and Meixner, F.X., 2002. Stability dependence of the relaxed eddy accumulation coefficient for various scalar quantities. *J. Geophys. Res. Atmos.*, 107(D8), 4071, doi: 10.1029/2001JD000649.

Atkinson, R., 1990. Gas-phase tropospheric chemistry of organic-compounds – a review. *Atmospheric Environment Part a – General Topics*, 24(1): 1-41.

Andreas, E.L. et al., 1998. Stability dependence of the eddy-accumulation coefficients for momentum and scalars. *Boundary-Layer Meteorol.*, 86(3): 409-420.

Badesha, S. S. (1999) *U.S. Patent No.5,999,781*. Washington, DC: U.S.

Baker, E.L., Smith, T.J., Landrigan, P.J., 1985. The neurotoxicity of industrial solvents – a review of the literature. *American Journal of Industrial Medicine*, 8(3): 207-217.

Baker, J.M., Norman, J.M. and Bland, W.L., 1992. Field-scale application of flux measurement by conditional sampling. *Ag. and For. Meteor.*, 62(1-2): 31-52.

Baker, A.K. et al., 2008. Measurements of nonmethane hydrocarbons in 28 United States cities. *Atmospheric Environment*, 42(1): 170-182.

Banta, R. M. et al., 2005. A bad air day in Houston. , *Bull. Am. Meteorol. Soc.*, 86(5): 657-669.

Bowling, D.R. et al., 1998. The use of relaxed eddy accumulation to measure biosphereatmosphere exchange of isoprene and of her biological trace gases. *Oecologia*, 116(3): 306-315.

Businger, J.A. and Oncley, S.P., 1990. Flux measurement with conditional sampling. *Journal of Atmospheric and oceanic Technology*. 7(2): 349-352.

Ciccioli, P. et al., 2003. Relaxed eddy accumulation, a new technique for measuring emission and deposition fluxes of volatile organic compounds by capillary gas

chromatography and mass spectrometry. *Journal of Chromatography A*, 985(1-2): 283-296.

Daum, P.H. et al., 2003. A comparative study of O3 formation in the Houston urban and industrial plumes during the 2000 Texas air quality study. *Journal of Geophysical Research-Atmospheres*, 108(D23).

Daum, P.H. et al., 2004. Origin and properties of plumes of high ozone observed during the Texas 2000 Air Quality Study (TexAQS 2000). 109(D17).

Desjardins, R.L., 1972. A study of carbon-dioxide and sensible heat fluxes using the eddy correlation technique. PH.D. Dissertation, Cornell University, Ithica, NY.

Draper, T.H.J. and Bamiou, D.E., 2009. Auditory neuropathy in a patient exposed to xylenes: case report. *Journal of Laryngology and Otology*, 123(4): 462-465.

Gallagher, M.W. et al., 2000. Assessment of a relaxed eddy accumulation for measurements of fluxes of biogenic volatile organic compounds: study over arable crops and a mature beech forest. *Atmospheric Environment*, 34(18): 2887-2899.

Gilman, J.B. et al., 2013. Source signature of volatile organic compounds from oil and natural gas operations in northeastern Colorado. *Environ. Sci. Technol.* 47(3): 1297-1305.

Grimminger, J., Muha, K., 1995. Silicone surfactants for pentane blown rigid foam. *J. Cell. Plast.*, 31(1): 48-72.

Houston Regional Monitoring Network. *Houston Regional Monitoring Network Overview*. Retrieved from the Houston Regional Monitoring Network website: hrm.radian.com/houston/presentation/Overview.ppt

Henze, D.K. et al., 2008. Global modeling of secondary organic aerosol formation from aromatic hydrocarbons: high vs. low-yield pathways. *Atmospheric Chemistry and Physics*, 8(9): 2405-2420.

Katul, G.G., Finkelstein, P.L., Clarke, J.F. and Ellestad, T.G., 1996. An investigation of the conditional sampling method used to estimate fluxes of active, reactive, and passive scalars. *J. Appl. Meteorol*, 35(10): 1835-1845.

Kelly, J.L. et al., 2010. Aerosol speciation and mass prediction from toluene oxidation under high NOx conditions. Atmospheric Environment, 44(3): 361 – 369.

Kljun, N., 2004. Evaluation of Langrangian footprint model using data from wind tunnel convective boundary layer. *Ag. and For. Meteor.*, 127(3-4): 189-201.

Kljun, N. et al., 2003. Comparison of the Langrangian footprint model LPDM-B with an analytical footprint model. *Boundary-Layer Meteorology*, 106: 349-355.

Kljun, N., Rotach, M.W. and Schmid, H.P., 2002. A three-dimensional backward lagrangian footprint model for a wide range of boundary-layer stratifications. *Boundary-Layer Meteorology*, 103(2): 205-226.

Kormann, R. and Meixner, F.X., 2001. An analytical footprint model for non-neutral stratification. *Boundary-Layer Meteorology*, 99(2): 207-224.

Kota, S. H. et al., 2014. Estimation of VOC emission factors from flux measurements using a receptor model and footprint analysis. *Atmospheric Environment*, 82(0): 24-35.

Lamanna, M.S. and Goldstein, A.H., 1999. In situ measurements of C-2 – C-10 volatile organic compounds above a Sierra Nevada ponderosa pine plantation. *J. Geophys Res. Atmos.*, 104(D17): 21247-21262.

Langford, B., Davison, B., Nemitz, E. and Hewitt, C.N., 2009. Mixing ratios and eddy covariance flux measurements of volatile organic compounds from an urban canopy (Manchester, UK). *Atm. Chem. and Phys.*, 9(6): 1971-1987.

Langford, B. et al., 2010. Fluxes and concentrations of volatile organic compounds above central London, U.K. *Atm. Chem. and Phys.*, 10(2): 627-645.

McGaughey, G.R. et al., 2004. Analysis of motor vehicle emissions in a Houston tunnel during the Texas Air Quality Study 2000. *Atmospheric Environment*, 38(20): 3363-3372.

Mehlman, M.A., 1990. Dangerous properties of petroleum-refining products – carcinogenicity of motor fuels (gasoline). *Teratogenesis Carcinogenesis and Mutagenesis*, 10(5): 399-408.

Milne, R., Mennim, A. and Hargreaves, K., 2001. The value of the beta coefficient in the relaxed eddy accumulation method in terms of fourth-order moments. *Boundary Layer Meteorology*, 101(3): 359-373.

Nemitz, E., Hargreaves, K.J., McDonald, A.G., Dorsey, J.R. and Fowler, D., 2002. Meteorological measurements of the urban heat budget and CO2 emissions on a city scale. *Environ. Sci. Technol.*, 36(14): 3139-3146.

Olofsson, M., Ek-Olausson, B., Ljungstrom, E. and Langer, S., 2003. Flux of organic compounds from grass measured by relaxed eddy accumulation technique. *J. Environ. Monit.*, 5(6): 963-970.

Pataki, D. E., D. R. Bowling, J. R. Ehleringer, and J. M. Zobitz, 2006: High resolution atmospheric monitoring of urban carbon dioxide sources. *Geophys. Res. Lett.*, 33, L03813.

Park, C., Schade, G. W., Boedeker, I., 2010. Flux measurements of volatile organic compounds by the relaxed eddy accumulation method combined with a GC-FID system in urban Houston, Texas. *Atmospheric Environment*, 44(21-22): 2605-2614.

Rinne, J., Douffet, T., Prigent, Y. and Durand, P., 2008. Field comparison of disjunct and conventional eddy covariance techniques for trace gas flux measurements. *Environ. Pollut.*, 152(3): 630-635.

Roth, M., 2000. Review of atmospheric turbulence over cities. *Quarterly Journal of the Royal Meteorological Society*, 126(564): 941-990.

Schade, G.W. and Goldstein, A.H., 2001. Fluxes of oxygenated volatile organic compounds from a ponderosa pine plantation. *J. Geophys Res. Atmos.*, 106(D3): 3111-3123.

TCEQ Permit Number 19940. <https://webmail.tceq.state.tx.us/gw/webpub>.

United States Environmental Protection Agency. (2007, February). *Control of Hazardous Air Pollutants from Mobile Sources: Final Rule to Reduce Mobile Source Air Toxics*. Retrieved from the Environmental Protection Agency website: http://www.epa.gov/OMS/regs/toxics/420f07017.pdf

Velasco, E. et al., 2005. Flux measurements of volatile organic compounds from an urban landscape. *Geophysical Research Letters*, 32, L20802, doi: 10.1028/2005GL023356.

Velasco, E. et al., 2009. Eddy covariance flux measurements of pollutant gases in urban Mexico City. *Atm. Chem. and Phys.*, 19: 7325-7342.

Vlasenko, A. et al., 2009 Measurements of VOCs by proton transfer reaction mass spectrometry at a rural Ontario Site: Sources and correlation to aerosol composition. *J. Geophys Res. Atmos.*, 114, D21305, doi:10.1029/2009JD012025.

Vizuete, W., Harvey, J.E., Tesche, T.W., 2011. Issues with ozone attainment methodology for Houston, Tx. *J Air Wast Manage Assoc*. 61(3): 238-253.

Von Schneidemesser, E. Paul, M.S., Plass-Duelmer, C., 2010. Global comparison of VOC and CO observations in urban areas. *Atmos. Environ.* 44(39): 5053-5064.

Warneke, C. et al., 2002. Disjunct eddy covariance measurements of oxygenated volatile organic compounds fluxes from an alfalfa field before and after cutting. *J. Geophys Res. Atmos.*, 107(D8), 4067, 10.1029/2001JD000594.

Warneke, C. et al., 2012. Multiyear trends in volatile organic compounds in Los Angeles, California: Five decades of decreasing emissions. *J. Geophys Res. Atmos.*, 117(D21): 2156-2202.

Whitworth, K.W., Symanski, E. and Coker, A.L., 2008 Childhood lymphohematopoietic cancer incidence and hazardous air pollutants in southeast Texas, 1995-2004. *Environmental Health Perspectives*, 116(11): 1576-1580.